Издательство ИТПЭ РАН

ISSN 2949-0553

СОВРЕМЕННАЯ ЭЛЕКТРОДИНАМИКА

научный рецензируемый журнал

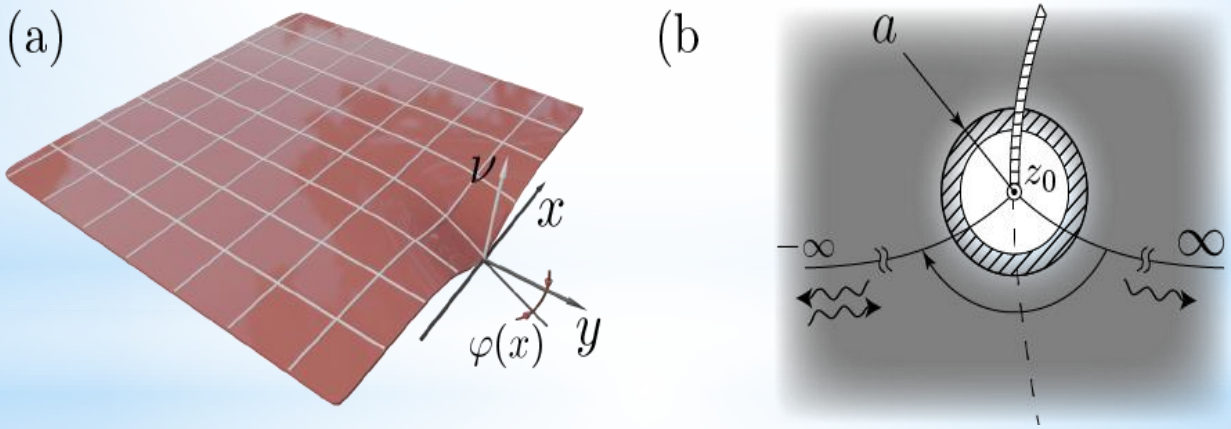

SCATTERING DUE TO EDGE IMPERFECTIONS IN TOPOLOGICAL INSULATORS IN THE UNIFORM MAGNETIC FIELD

Ya. I. Rodionov

2024 № 5 (13)

Федеральное государственное бюджетное учреждение науки
Институт теоретической и прикладной электродинамики
Российской академии наук

Журнал основан в 2022 году

Выпуск № 5 (13)

Современная электродинамика

научный рецензируемый журнал

Под редакцией академика РАН А.Н. Лагарькова

Москва, 2024

Федеральное государственное бюджетное учреждение науки

Институт теоретической и прикладной электродинамики Российской академии наук

ISSN 2949-0553

Современная электродинамика

Научный рецензируемый журнал. Издаётся с октября 2022 года.

Выходит один раз в два месяца.

№ 5 (13)

2024

Адрес редакции:

125412, г. Москва, ул. Ижорская, д.13, стр. 6

тел., факс 8 (495) 484-26-33

эл.почта electrodynamics@mail.ru

Зав. редакцией Е.В. Зеневич

Компьютерная вёрстка: Е.В. Зеневич

Свидетельство о регистрации Эл № ФС77-83666 от 26.07.2022 г.

Подписано в печать 19.11.2024. Тираж 30 экз.

Содержание номера

УДК 535.016

ПОВЕРХНОСТНАЯ ДИЭЛЕКТРИЧЕСКАЯ ПРОНИЦАЕМОСТЬ СВЕРХТОНКИХ СЛОЁВ

Д.К. Высоких * [1,2,3], А.А. Пухов[1,3], Д.П. Куликова[2], А.Ш. Амирасланов[4], А.В. Барышев[2], А.С. Бабурин[2,4], И.А. Родионов[2,4], А.В. Дорофеенко[1,2,3]

[1] *Федеральное государственное бюджетное учреждение науки Институт теоретической и прикладной электродинамики Российской академии наук, Москва, Россия*
[2] *Федеральное государственное унитарное предприятие "Всероссийский научно-исследовательский институт автоматики им. Н.Л. Духова", Москва, Россия*
[3] *Федеральное государственное автономное образовательное учреждение высшего образования "Московский физико-технический институт (национальный исследовательский университет)", Москва, Россия*
[4] *Московский государственный технический университет имени Н.Э. Баумана (национальный исследовательский университет), Москва, Россия*

Статья поступила в редакцию 24.10.2024
Одобрена после рецензирования 06.11.2024
Принята к публикации 19.11.2024

Аннотация

В различных оптических устройствах часто применяют слои с толщиной, много меньшей длины волны. Такие слои могут использоваться в качестве просветляющих плёнок, поглотителей, катализаторов или функциональных покрытий. Для расчёта оптических систем, содержащих сверхтонкие слои, важно развить их корректное описание, включающее необходимый минимум электродинамических параметров. Мы предлагаем описание произвольного неоднородного сверхтонкого слоя с помощью поверхностной диэлектрической проницаемости κ, не требующее знания толщины слоя. При этом мы показываем, что κ есть скалярная комплексная величина, т.е. предложенный подход не включает в себя рассмотрение анизотропных свойств слоя. Для подтверждения предложенного метода мы проводим обработку измеренных спектров эллипсометрии и показываем, что описание слоя с помощью κ не увеличивает существенно погрешность по сравнению с описанием через однородный слой конечной толщины, но при этом уменьшает число параметров модели, делая её более удобной для применения. Помимо этого, мы находим связь параметра κ с широко используемой при описании тонких слоёв величиной – сопротивлением на квадрат.

Ключевые слова: сверхтонкие плёнки, эллипсометрия, комплексный показатель преломления, оптические константы

EDN YTQUYD

doi:10.24412/2949-0553-2024-513-04-13

1. Введение

Одной из важных задач оптики тонких плёнок является задача определения их оптических характеристик. Основной оптической характеристикой служит комплексная диэлектрическая проницаемость, которая в макроскопическом приближении описывает взаимодействие электромагнитной волны с веществом. С одной стороны, знание комплексной диэлектрической проницаемости используется в исследовании материалов в таких областях, как фотовольтаика, фотолюминесценция и физика полупроводников [1, 2]. С другой стороны, оптические характеристики плёнок необходимы для проектирования различных устройств [3].

Для определения оптических характеристик тонких плёнок широко используется спектроскопическая эллипсометрия [1, 2, 4–7]. В отличие от методов, основанных на измерении мощности сигнала, таких как спектроскопия пропускания, отражения и поглощения [8–10], в которых измеряются амплитудные коэффициенты, эллипсометрия также измеряет *разность фаз* коэффициентов отражения для двух поляризаций, что даёт дополнительную информацию об объекте [4]. Традиционный эллипсометрический

*Автор, ответственный за переписку: Дмитрий Константинович Высоких, vysokikh.dk@phystech.edu

анализ подразумевает расчёт эллипсометрических параметров ψ, Δ в зависимости от диэлектрической проницаемости и приведение этих параметров в соответствие с экспериментальными данными путём её вариации [5]. Эта процедура хорошо отлажена для различных диэлектрических и металлических плёнок достаточно большой, сравнимой с длиной волны толщины.

Однако для сверхтонких плёнок, т.е. пленок толщиной менее 10 нм, определение адекватных значений толщины и диэлектрической проницаемости затруднительно [11–16]. Это в первую очередь связано с сильной корреляцией между этими двумя величинами, которые в случае сверхтонких плёнок изменяются обратно пропорционально друг другу [11,12]. Как правило, сверхтонкие слои моделируются как некие однородные слои с толщиной, определяемой с помощью минимизации невязки [5,6,8–10,17,18]. Однако во многих случаях слой не является сплошным или шероховатость подложки сравнима с его толщиной. Возникает вопрос о физическом смысле толщины такого слоя. Кроме того, минимум невязки обычно оказывается недостаточно резким, что приводит к существенной ошибке при определении толщины слоя. Поэтому требуется иное описание сверхтонких плёнок, не использующее плохо определённый параметр – толщину плёнки.

В данной работе предложено такое описание. Вводится поверхностная диэлектрическая проницаемость, позволяющая характеризовать взаимодействие плёнки с излучением любой поляризации, падающим под произвольным углом. Применимость подхода проверена сравнением с экспериментальными данными. Проведено сравнение стандартного описания слоем конечной толщины с предложенным здесь подходом.

2. Описание сверхтонкого слоя T-матрицами

В качестве достаточно общей постановки задачи рассмотрим прохождение плоской волны через неоднородный тонкий слой, находящийся между двумя диэлектриками, под произвольным углом (рис. 1). Направим ось z перпендикулярно слою, ось x – параллельно слою, так чтобы xz была плоскостью падения.

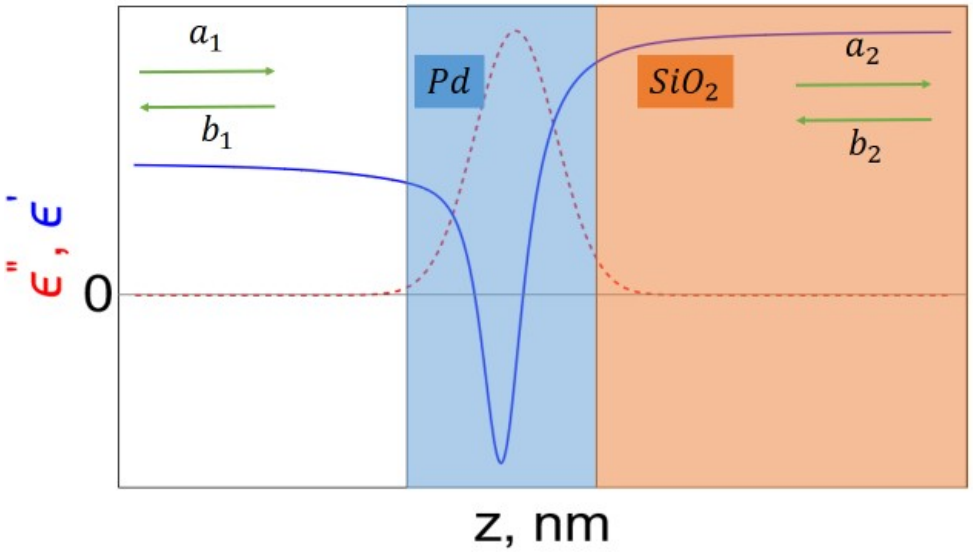

Рисунок 1 – Геометрия рассматриваемой системы и схематический вид пространственной зависимости мнимой и действительной частей диэлектрической проницаемости. Для s-поляризации a_1, b_1 – комплексные амплитуды электрического поля волн слева от слоя, a_2, b_2 – справа от слоя. Для p-поляризации a_1, b_1 – комплексные амплитуды магнитного поля волн слева от слоя, a_2, b_2 – справа от слоя

Для расчёта многослойных систем, как правило, используется метод T-матриц [19, 20]. Вид T-матрицы зависит от поляризации, т.е. различен для s- и p-поляризованных волн. Рассмотрим оба возможных варианта.

Начнём с ***s*-поляризации**. Уравнение Гельмгольца имеет вид:

$$\frac{d^2E}{dz^2} + \left(k_0^2\varepsilon\left(z\right) - k_x^2\right)E = 0. \tag{1}$$

При условии малой толщины слоя оно даёт следующие граничные условия:

$$E\left(+0\right) = E\left(-0\right) \tag{2}$$

и

$$\frac{dE}{dz}(+0) - \frac{dE}{dz}(-0) + k_0^2 E(0) \int \varepsilon dz = 0. \tag{3}$$

Таким образом, слой может быть охарактеризован *безразмерной* поверхностной диэлектрической проницаемостью $\kappa = k_0 \int \varepsilon dz$.

Уравнения (2) и (3) представляют собой правила сшивки для s-поляризации, которое можно переписать через комплексные амплитуды электрического поля волн, распространяющихся вправо и влево, слева от слоя $(a_1,\, b_1)$ и справа от слоя $(a_2,\, b_2)$:

$$a_1 + b_1 = a_2 + b_2, \tag{4}$$

$$ik_2(a_2 - b_2) - ik_1(a_1 - b_1) + k_0\kappa(a_1 + b_1 + a_2 + b_2)/2 = 0. \tag{5}$$

Чтобы составить матрицу прохождения через слой, запишем систему уравнений для a_2 и b_2:

$a_2(ik_2 + k_0\kappa/2) + b_2(-ik_2 + k_0\kappa/2) = ik_1(a_1 - b_1) - k_0\kappa(a_1 + b_1)/2,$

$a_1 + b_1 = a_2 + b_2.$

Детерминант этой системы:

$\det = (ik_2 + k_0\kappa/2) - (-ik_2 + k_0\kappa/2) = 2ik_2,$

откуда нетрудно получить:

$a_2 = [a_1(k_1 + k_2 + ik_0\kappa) + b_1(-k_1 + k_2 + ik_0\kappa)]/(2k_2)$

$b_2 = [a_1(-k_1 + k_2 - ik_0\kappa) + b_1(k_1 + k_2 - ik_0\kappa)]/(2k_2)$

Соответствующая матрица задаётся выражением:

$$S(s) = \frac{1}{2k_2}\begin{pmatrix} k_2 + k_1 + ik_0\kappa & k_2 - k_1 + ik_0\kappa \\ k_2 - k_1 - ik_0\kappa & k_2 + k_1 - ik_0\kappa \end{pmatrix} \tag{6}$$

Введём обозначение для адмиттанса: $Z_i = k_i/k_0$. Тогда:

$$S(s) = \frac{1}{2Z_2}\begin{pmatrix} Z_2 + Z_1 + i\kappa & Z_2 - Z_1 + i\kappa \\ Z_2 - Z_1 - i\kappa & Z_2 + Z_1 - i\kappa \end{pmatrix}. \tag{7}$$

Рассмотрим теперь ***p*-поляризацию**. Для неё уравнение Гельмгольца имеет вид

$$\frac{d}{dz}\frac{1}{\varepsilon(z)}\frac{dH}{dz} + \left(k_0^2 - \frac{k_x^2}{\varepsilon(z)}\right)H = 0. \tag{8}$$

Первое граничное условие, связанное с непрерывностью тангенциальной компоненты электрического поля, имеет вид

$$\left(\frac{1}{\varepsilon(z)}\frac{dH}{dz}\right)(-0) = \left(\frac{1}{\varepsilon(z)}\frac{dH}{dz}\right)(+0). \tag{9}$$

Второе граничное условие, описывающее скачок магнитного поля, имеет вид

$$H(+0) - H(-0) = \int\limits_{-0}^{+0} \frac{dH}{dz} dz = \int\limits_{-0}^{+0} \frac{1}{\varepsilon}\frac{dH}{dz}\varepsilon dz = \left(\frac{1}{\varepsilon}\frac{dH}{dz}\right)\int\limits_{-0}^{+0} \varepsilon dz.$$

Таким образом,

$$H(+0) - H(-0) = \frac{\kappa}{k_0}\left(\frac{1}{\varepsilon}\frac{dH}{dz}\right). \tag{10}$$

Заметим, что характеристикой слоя как для s-, так и для p-поляризации служит величина κ.

Для p-поляризации условие сшивки записывается через комплексные амплитуды магнитного поля волн, распространяющихся вправо и влево, слева от слоя $(a_1,\, b_1)$ и справа от слоя $(a_2,\, b_2)$:

$$i\frac{k_1}{\varepsilon_1}(a_1 - b_1) = i\frac{k_2}{\varepsilon_2}(a_2 - b_2), \tag{11}$$

$$(a_2 + b_2) - (a_1 + b_1) = \frac{\kappa}{2k_0}\left[\frac{ik_1}{\varepsilon_1}(a_1 - b_1) + \frac{ik_2}{\varepsilon_2}(a_2 - b_2)\right]. \tag{12}$$

Для составления матрицы прохождения через слой перепишем систему уравнений в виде:

$$a_2 - b_2 = \frac{\varepsilon_2 k_1}{\varepsilon_1 k_2}\left(a_1 - b_1\right), \tag{13}$$

$$a_2\left(1 - \frac{\kappa}{2k_0}\frac{ik_2}{\varepsilon_2}\right) + b_2\left(1 + \frac{\kappa}{2k_0}\frac{ik_2}{\varepsilon_2}\right) = a_1\left(1 + \frac{\kappa}{2k_0}\frac{ik_1}{\varepsilon_1}\right) + b_1\left(1 - \frac{\kappa}{2k_0}\frac{ik_1}{\varepsilon_1}\right). \tag{14}$$

Детерминант системы уравнений (13), (14) равен 2, откуда нетрудно получить:

$$a_2 = \tfrac{a_1}{2}\left[1 + \tfrac{\varepsilon_2 k_1}{\varepsilon_1 k_2} + i\tfrac{\kappa}{k_0}\tfrac{k_1}{\varepsilon_1}\right] + \tfrac{b_1}{2}\left[1 - \tfrac{\varepsilon_2 k_1}{\varepsilon_1 k_2} - i\tfrac{\kappa}{k_0}\tfrac{k_1}{\varepsilon_1}\right],$$

$$b_2 = \tfrac{a_1}{2}\left[1 - \tfrac{\varepsilon_2 k_1}{\varepsilon_1 k_2} + \tfrac{\kappa}{k_0}\tfrac{ik_1}{\varepsilon_1}\right] + \tfrac{b_1}{2}\left[1 + \tfrac{\varepsilon_2 k_1}{\varepsilon_1 k_2} - \tfrac{\kappa}{k_0}\tfrac{ik_1}{\varepsilon_1}\right].$$

Обозначив импедансы $Z_i = k_i/k_0\varepsilon_i$, запишем матрицу прохождения через слой:

$$S\left(p\right) = \frac{1}{2Z_2}\begin{pmatrix} Z_2 + Z_1 + i\kappa Z_1 Z_2 & Z_2 - Z_1 - i\kappa Z_1 Z_2 \\ Z_2 - Z_1 + i\kappa Z_1 Z_2 & Z_2 + Z_1 - i\kappa Z_1 Z_2 \end{pmatrix}. \tag{15}$$

Таким образом, процессы отражения и пропускания волн обеих поляризаций могут быть полностью описаны с помощью поверхностной диэлектрической проницаемости

$$\kappa = k_0 \int \varepsilon dz. \tag{16}$$

Часто свойства сверхтонких проводящих слоёв описываются с использованием такого параметра, как сопротивление на квадрат:

$$R = 1/\left(\sigma d\right), \tag{17}$$

где d – толщина слоя, σ – объёмная проводимость, которая связана с мнимой частью диэлектрической проницаемости ε'' соотношением $\varepsilon_0\varepsilon'' = \sigma/\omega$, т.е.

$$\sigma = \varepsilon_0\varepsilon''\omega. \tag{18}$$

Здесь использована запись в системе СИ, чтобы сопротивление измерялось в единицах Ом. Тогда, учитывая выражения (17) и (18), имеем $R = 1/\left(\varepsilon_0\varepsilon''\omega d\right) = 1/\left(c\varepsilon_0\kappa''\right)$. Поскольку $1/\left(c\varepsilon_0\right) = Z_0$ есть импеданс вакуума, получим соотношение

$$R = Z_0/\kappa''. \tag{19}$$

Таким образом, действительное значение сопротивления на квадрат выражается через мнимую часть поверхностной диэлектрической проницаемости.

Заметим, что малым параметром в нашем подходе является величина $k_0 d\sqrt{\varepsilon}$, которая связана с поверхностной диэлектрической проницаемостью соотношением $k_0 d\sqrt{\varepsilon} = \kappa/\sqrt{\varepsilon}$. В частности, в приведённом ниже расчёте для палладиевой плёнки величина $k_0 d\sqrt{\varepsilon}$ оказывается меньше 0.1, тогда как κ принимает значения порядка единицы.

3. Верификация метода посредством сравнения с экспериментальными данными

Была проведена оценка применимости описания сверхтонких слоёв поверхностной диэлектрической проницаемостью путём обработки экспериментальных данных. Для этого были изготовлены образцы сверхтонких плёнок палладия на стеклянных подложках методом электронно-лучевого напыления. Часть образцов подверглась отжигу при температуре 600 С.

Полученные в эксперименте данные были обработаны двумя способами: с помощью описания плёнки палладия слоем конечной толщины и поверхностной диэлектрической проницаемостью.

3.1. Обработка с использованием описания системы слоем конечной толщины

Экспериментальные данные для численной обработки были получены из эллипсометрических измерений параметров ψ, Δ (далее совместно приведены данные для слоя палладия с отжигом и без отжига). Эллипсометрия снималась при углах падения 45, 60 и 75 °.

В ходе обработки экспериментальных данных была произведена минимизация функции невязки, зависящей от расчётного эллипсометрического параметра $\rho_{theor} = r_p/r_s$, представляющего собой отношение комплексных амплитуд отражённых волн s- и p-поляризаций: этот параметр $\rho_{theor}(\lambda, \theta, \varepsilon, d)$ зависит от длины волны падающего излучения λ, угла падения θ, диэлектрической проницаемости ε и толщины исследуемого слоя d. Таким образом, невязка равна

$$f(\lambda, \varepsilon, d) = \sum_{\theta} |\rho_{theor}(\lambda, \theta, \varepsilon, d) - \rho_{exp}(\lambda, \theta)|^2. \tag{20}$$

Здесь $\rho_{exp} = \mathrm{tg}\psi \exp(-i\Delta)$.

В результате поточечной минимизации функции невязки по длинам волн при фиксированной толщине слоя ($d = 7$ нм) была найдена дисперсионная зависимость $\varepsilon(\lambda)$, доставляющая невязке минимум (рис. 2).

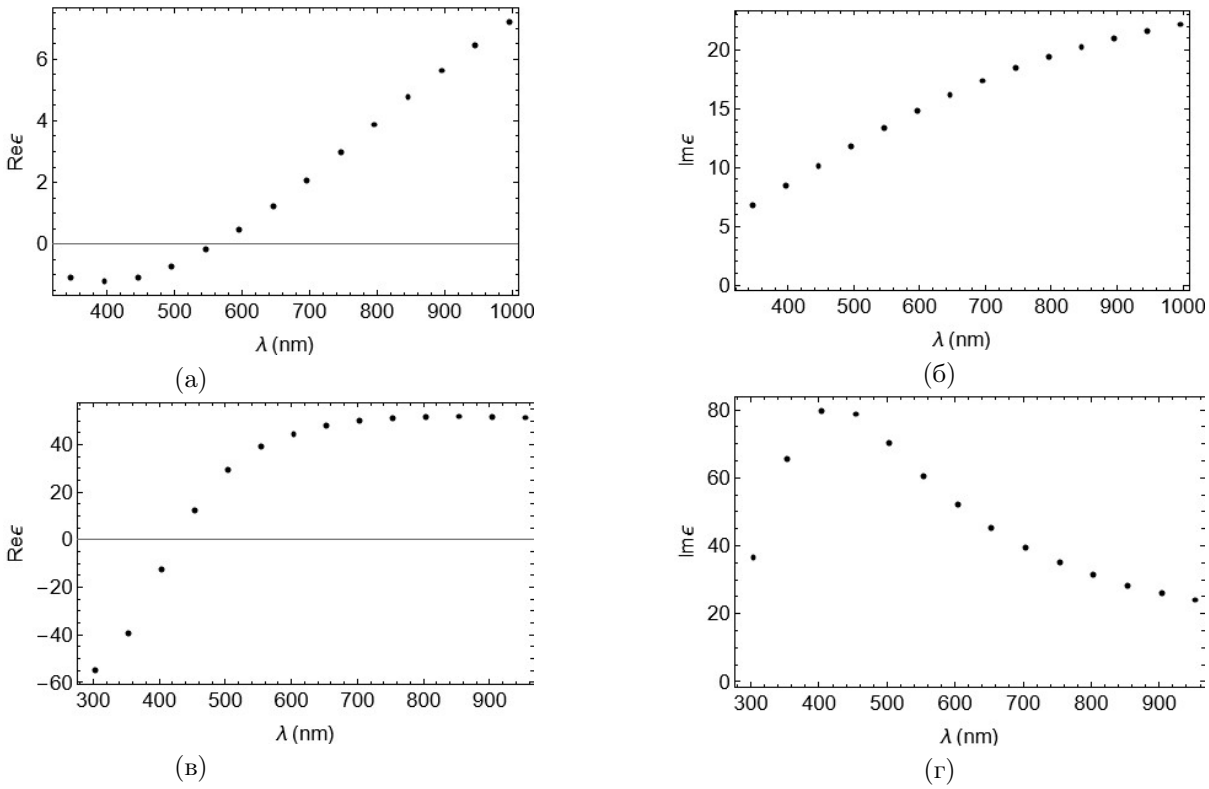

Рисунок 2 – Зависимость действительной (левый столбец) и мнимой (правый столбец) частей диэлектрической проницаемости от длины волны. Толщина слоя выбрана равной $d = 7$ нм для палладия без отжига (верхняя строка) и $d = 0.3$ нм для палладия с отжигом (нижняя строка), что соответствует минимуму невязки

В предыдущих рассуждениях при минимизации функции невязки толщина слоя была фиксирована ($d = 7$ нм). Для нахождения же толщины слоя, минимизирующей невязку, построим новую функцию невязки, зависящую только от толщины. Для этого будем минимизировать значение невязки по ε и суммировать по всем длинам волн:

$$F(d) = \sum_{\lambda} \min_{\varepsilon} f(\lambda, \varepsilon, d) \tag{21}$$

Оказалось, что полученная суммарная величина (21) имеет минимум при некотором значении толщины слоя (рис. 3).

Из полученной зависимости $\varepsilon(\lambda)$ при фиксированном параметре $d = 7$ нм были рассчитаны эллипсометрические параметры ψ и Δ, которые находятся в хорошем соответствии с исходными экспериментальными данными (рис. 4).

3.2. Обработка с использованием поверхностной диэлектрической проницаемости

Далее была произведена численная обработка тех же данных с помощью описания сверхтонкого слоя поверхностной диэлектрической проницаемостью κ. Заметим, что расчётный эллипсометрический

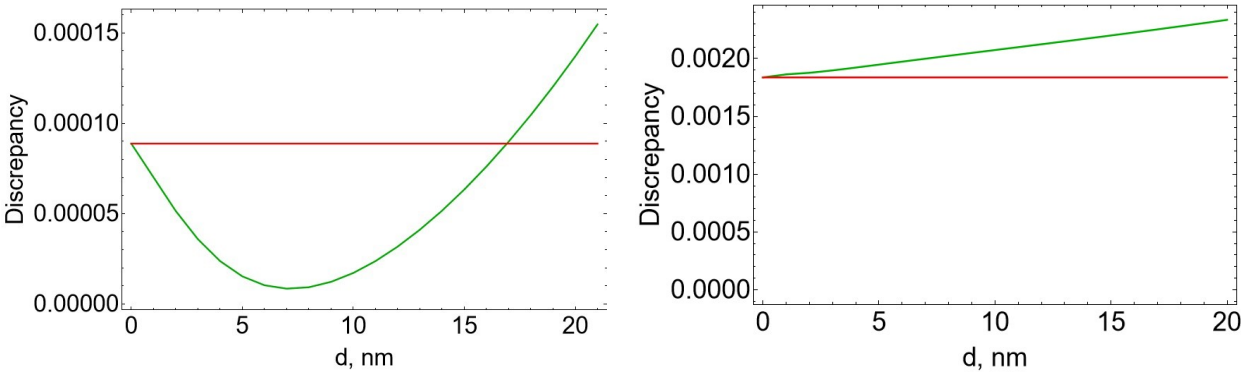

(а) (б)

Рисунок 3 – Зависимость невязки, суммированной по различным значениям длины волны, от толщины палладиевого слоя (зелёные кривые) и не зависящее от толщины значение невязки, рассчитанной через параметр тонкого слоя (красные горизонтальные линии) а) для палладия без отжига, б) для палладия с отжигом

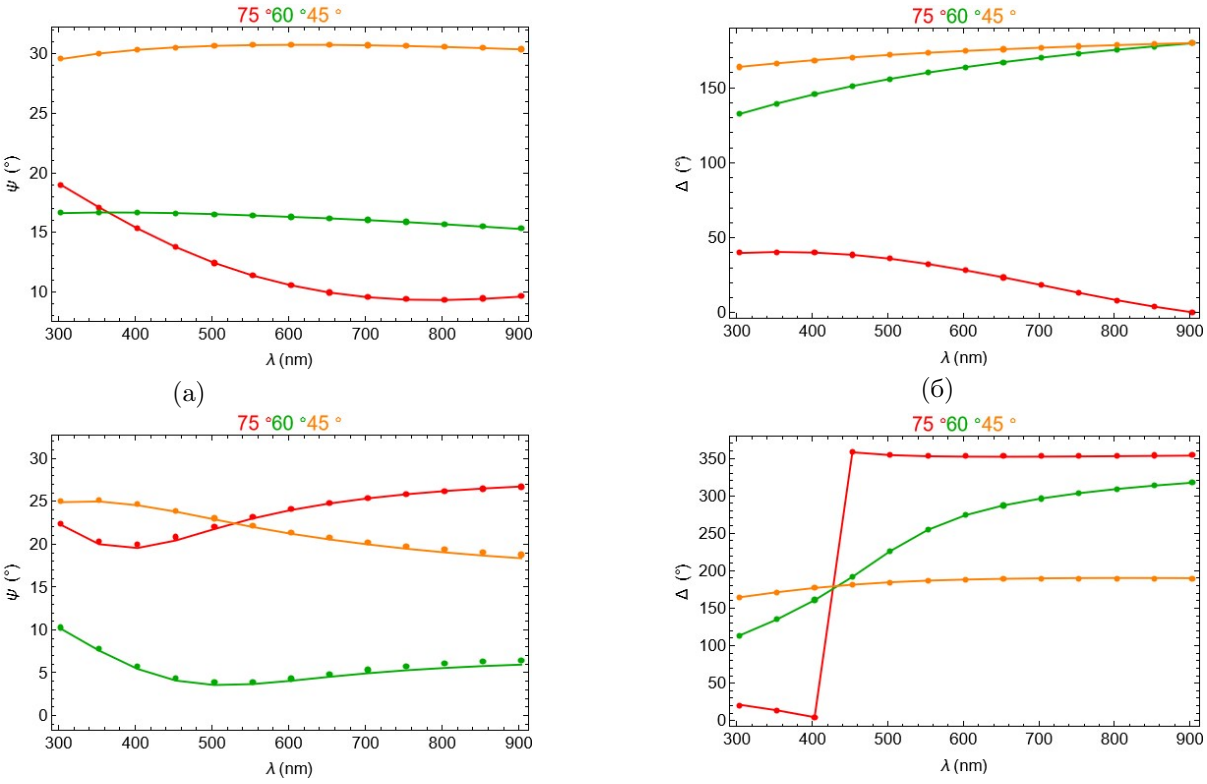

(а) (б)

(в) (г)

Рисунок 4 – Значения эллипсометрических параметров ψ (левый столбец) и Δ (правый столбец), найденные теоретически (кривые) и полученные экспериментально (точки), для разных углов падения (показаны цветом): для палладия без отжига (верхняя строка) и для палладия с отжигом (нижняя строка)

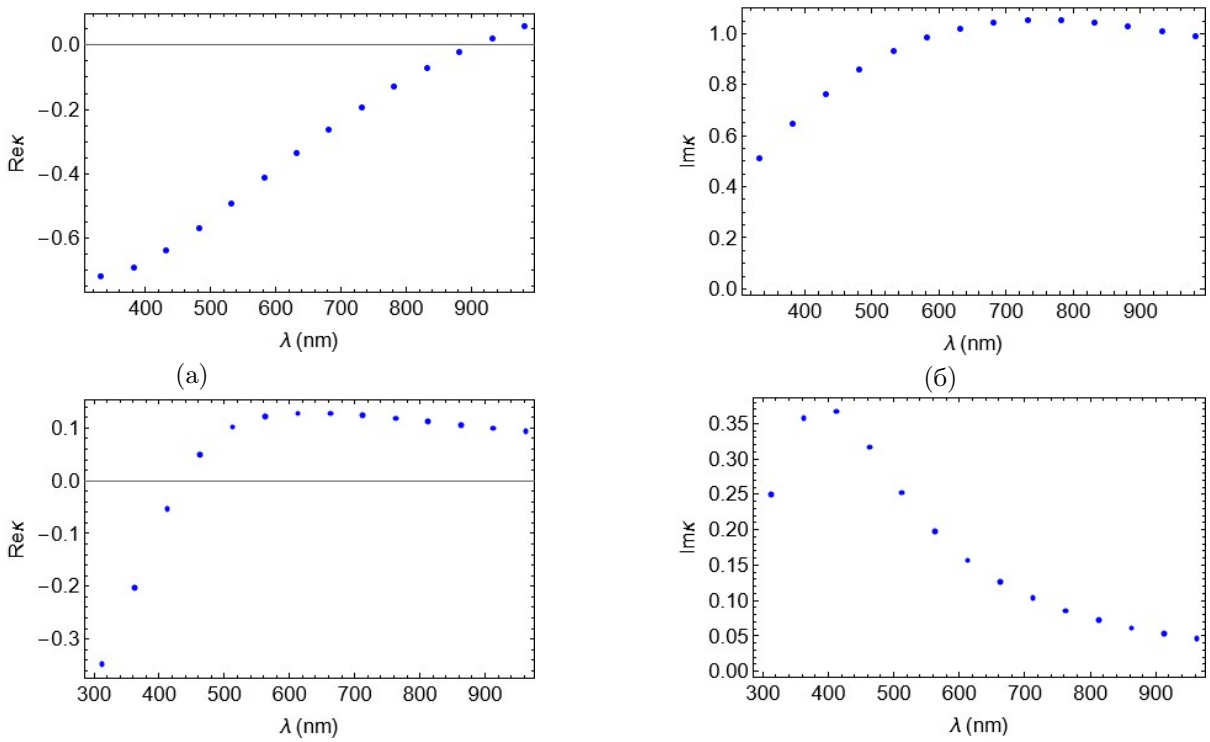

Рисунок 5 – Зависимость действительной (левый столбец) и мнимой (правый столбец) частей параметра κ от длины волны λ = 300–1 000 нм для палладия без отжига (верхняя строка) и палладия с отжигом (нижняя строка)

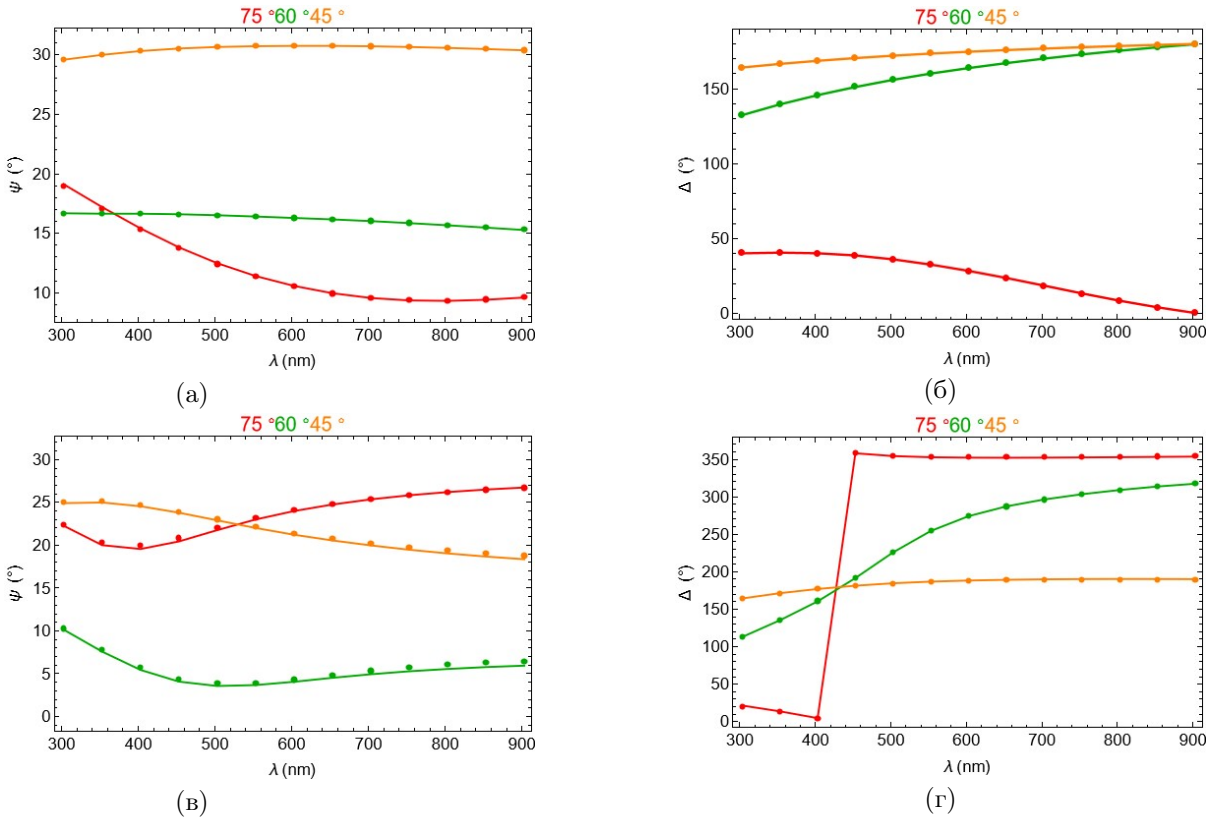

Рисунок 6 – Значения эллипсометрических параметров ψ (левый столбец) и Δ (правый столбец), найденные теоретически (кривые) и полученные экспериментально (точки), для разных углов падения (показаны цветом): для палладия без отжига (верхняя строка) и палладия с отжигом (нижняя строка)

параметр при таком подходе зависит от длины волны падающего излучения λ, угла падения θ и значения поверхностной диэлектрической проницаемости κ: $\rho_{theor}(\lambda, \theta, \kappa)$. При этом параметр ρ, как и функция невязки, не зависит от толщины слоя:

$$f(\lambda, \kappa) = \sum_{\theta} |\rho_{theor}(\lambda, \theta, \kappa) - \rho_{exp}(\lambda, \theta)|^2. \tag{22}$$

В результате поточечной минимизации функции невязки при каждой длине волны была найдена дисперсионная зависимость $\kappa(\lambda)$, доставляющая невязке минимум (рис. 5). Из полученной зависимости $\kappa(\lambda)$ были рассчитаны эллипсометрические параметры ψ и Δ, которые также находятся в хорошем соответствии с параметрами, найденными экспериментально (рис. 6).

Суммированная по длинам волн невязка

$$F = \sum_{\lambda} \min_{\kappa} f(\lambda, \kappa), \tag{23}$$

найденная при описании электродинамических свойств тонкого слоя посредством параметра κ, не зависит от толщины слоя. Для удобства сравнения с предыдущими результатами величина этой суммарной невязки отмечена на рис. 3.

Можно заметить, что описание, использующее параметр тонкого слоя κ, даёт несколько большую погрешность по сравнению со стандартным описанием (раздел 3.1), однако это компенсируется простотой использования данного подхода, а также отсутствием в нём избыточных параметров.

4. Заключение

Был предложен качественно новый подход к описанию электромагнитных свойств сверхтонких слоёв, основанный на использовании поверхностной диэлектрической проницаемости вместо объёмной. Основное преимущество данного метода состоит в том, что он не требует учёта такого трудно интерпретируемого параметра, как толщина сверхтонкого слоя, и, как следствие, более удобен для применения на практике. Более того, отсутствие лишних параметров снижает склонность метода к «переобучению». Применимость данного метода продемонстрирована на примере обработки эллипсометрических данных для сверхтонких палладиевых плёнок как с отжигом при температуре 600 °C, так и без отжига. В обоих случаях получено хорошее совпадение значений эллипсометрических параметров ψ и Δ, полученных из эксперимента и найденных теоретически при помощи минимизации функции невязки. Несмотря на то, что классический подход к описанию свойств сверхтонких слоёв даёт меньшую абсолютную ошибку при определении эллипсометрических параметров по сравнению с подходом, предложенным в нашей статье, простота и физическая обоснованность последнего дают основание полагать, что он имеет большие перспективы для широкого практического применения.

Список литературы

[1] Shirayama M., Kadowaki H., Miyadera T., Sugita T., Tamakoshi M., Kato M., Fujiseki T., Murata D., Hara S., Murakami T. N. Optical transitions in hybrid perovskite solar cells: ellipsometry, density functional theory, and quantum efficiency analyses for $CH_3NH_3PbI_3$ // Physical Review Applied. – 2016. – V. 5. – N 1. – P. 014012.

[2] Zhao M., Shi Y., Dai J., Lian J. Ellipsometric study of the complex optical constants of a $CsPbBr_3$ perovskite thin film // Journal of Materials Chemistry C. – 2018. – V. 6. – N 39. – P. 10450-10455.

[3] Ke X., Gu H., Zhao X., Chen X., Shi Y., Zhang C., Jiang H., Liu S. Simulation method for study on outcoupling characteristics of stratified anisotropic OLEDs // Optics Express. – 2019. – V. 27. – N 16. – P. A1014-A1029.

[4] Xia R., Gu H., Liu S., Zhang K., Yip H. L., Cao Y. Optical analysis for semitransparent organic solar cells // Solar RRL. – 2019. – V. 3. – N 1. – P. 1800270.

[5] Fujiwara H. Spectroscopic Ellipsometry: Principles and Applications. – Hoboken: John Wiley & Sons, 2007.

[6] Song B., Gu H., Zhu S., Jiang H., Chen X., Zhang C., Liu S. Broadband optical properties of graphene and HOPG investigated by spectroscopic Mueller matrix ellipsometry // Applied Surface Science. – 2018. – V. 439. – P. 1079-1087.

[7] Song B., Gu H., Fang M., Ho Y.-T., Chen X., Jiang H., Liu S. Complex optical conductivity of two-dimensional MoS_2: A striking layer dependency // The Journal of Physical Chemistry Letters. – 2019. – V. 10. – N 20. – P. 6246-6252.

[8] Gu H., Song B., Fang M., Hong Y., Chen X., Jiang H., Ren W., Liu S. Layer-dependent dielectric and optical properties of centimeter-scale 2D WSe 2: evolution from a single layer to few layers // Nanoscale. – 2019. – V. 11. – N 47. – P. 22762-22771.

[9] Brindza M., Flynn R. A., Shirk J. S., Beadie G. Thin sample refractive index by transmission spectroscopy // Optics Express. – 2014. – V. 22. – N 23. – P. 28537-28552.

[10] Hoffman A. J., Alekseyev L., Howard S. S., Franz K. J., Wasserman D., Podolskiy V. A., Narimanov E. E., Sivco D. L., Gmachl C. Negative refraction in semiconductor metamaterials // Nature materials. – 2007. – V. 6. – N 12. – P. 946-950.

[11] Gray A., Balooch M., Allegret S., De Gendt S., Wang W.-E. Optical detection and characterization of graphene by broadband spectrophotometry // Journal of Applied Physics. – 2008. – V. 104. – N 5.

[12] Tompkins H. G., Hilfiker J. N. Spectroscopic ellipsometry: practical application to thin film characterization. – New York: Momentum Press, 2015.

[13] Arwin H. Adsorption of proteins at solid surfaces // Ellipsometry of Functional Organic Surfaces and Films. – 2014. – P. 29-46.

[14] Arwin H., Aspnes D. E. Unambiguous determination of thickness and dielectric function of thin films by spectroscopic ellipsometry // Thin Solid Films. – 1984. – V. 113. – N 2. – P. 101-113.

[15] Gordan O. D., Zahn D. R. Small organic molecules // Ellipsometry of Functional Organic Surfaces and FilmsSpringer, 2014. – C. 197-219.

[16] Richter R. P., Rodenhausen K. B., Eisele N. B., Schubert M. Coupling spectroscopic ellipsometry and quartz crystal microbalance to study organic films at the solid-liquid interface // Ellipsometry of Functional Organic Surfaces and Films. – 2014. – P. 223-248.

[17] Kulikova D. P., Dobronosova A. A., Kornienko V. V., Nechepurenko I. A., Baburin A. S., Sergeev E. V., Lotkov E. S., Rodionov I. A., Baryshev A. V., Dorofeenko A. V. Optical properties of tungsten trioxide, palladium, and platinum thin films for functional nanostructures engineering // Optics express. – 2020. – V. 28. – N 21. – P. 32049-32060.

[18] Song B., Gu H., Fang M., Chen X., Jiang H., Wang R., Zhai T., Ho Y. T., Liu S. Layer-dependent dielectric function of wafer-scale 2D MoS_2 // Advanced Optical Materials. – 2019. – V. 7. – N 2. – P. 1801250.

[19] Hao J., Zhou L. Electromagnetic wave scatterings by anisotropic metamaterials: Generalized $4\times$ 4 transfer-matrix method // Physical Review B—Condensed Matter and Materials Physics. – 2008. – V. 77. – N 9. – P. 094201.

[20] Katsidis C. C., Siapkas D. I. General transfer-matrix method for optical multilayer systems with coherent, partially coherent, and incoherent interference // Applied optics. – 2002. – V. 41. – N 19. – P. 3978-3987.

SURFACE PERMITTIVITY OF ULTRATHIN FILMS

D.K. Vysokikh[*1,2,3], A.A. Pukhov[1,3], D.P. Kulikova[2], A.S Amiraslanov[4], A.V. Baryshev[2], A.S. Baburin[2,4], I.A. Rodionov[2,4], A.V. Dorofeenko[1,2,3]

[1] Institute for Theoretical and Applied Electromagnetics of RAS, Moscow, Russia
[2] Dukhov Research Institute of Automatics, Moscow, Russia
[3] Moscow Institute of Physics and Technologies, Moscow, Russia
[4] Bauman Moscow State Technical University, Moscow, Russia

[*] vysokikh.dk@phystech.edu

Abstract

Slabs of width much smaller than the wavelength are of high importance in many areas of electrodynamics. Such slabs are widely used as antireflection films, absorbers, catalysts and functional coatings. For treating optical systems involving ultrathin films, it is crucial to propose their proper description considering only necessary parameters. We provide a theoretical characterization of an arbitrary inhomogeneous ultrathin slab using surface permittivity κ, which does not require knowledge of the slab thickness. Moreover, we show that κ is a scalar complex value, i.e. the proposed approach does not include consideration of the anisotropic properties of the slab. We process experimentally measured ellipsometry spectra to confirm the reliability of proposed method. We also show that the description of the slab using κ does not significantly increase the discrepancy comparing to the description through a homogeneous layer of finite thickness, at the same time reducing the number of model parameters making it more convenient to use. In addition, we find a relation between the parameter κ and the resistance per square widely used in the description of thin conducting layers.

Key words: ultrathin films, ellipsometry, complex refractive index, optical constants

УДК 538.915

SCATTERING DUE TO EDGE IMPERFECTIONS IN TOPOLOGICAL INSULATORS IN THE UNIFORM MAGNETIC FIELD

Rodionov Ya.I. * [1]

[1]Institute for Theoretical and Applied Electrodynamics, Russian Academy of Sciences, Moscow, Russia

Received: 23.09.2024
Accepted: 06.11.2024
Published: 19.11.2024

Abstract

We study the scattering of edge excitations of 2D topological insulator (TI) in the uniform external magnetic field due to edge imperfections, ubiquitous in realistic 2D TIs. Our previous study shows the possible existence of oscillations of reflection amplitude in a weak magnetic field. In this paper, we address yet another general class of edge deformation profiles and also discover quantum oscillations of the scattering coefficient in one more general situation of low momentum carriers. The semiclassical Pokrovsky-Khalatnikov approach is used to obtain reflection coefficient with pre-exponential accuracy.

Ключевые слова: Topological Insulators, semiclassical scattering

EDN JFUKPW

doi:10.24412/2949-0553-2024-513-14-24

1. Introduction

Topological insulators (TIs) are novel materials that cannot be continuously converted into semiconductors or conventional insulators. They are distinguished by gapless edge or surface states and a complete insulating gap in the bulk. Time reversal (TR) symmetry protects the edge (in 2D TIs) or surface (in 3D TIs) states from elastic scattering. Error-tolerant quantum computing [1, 2] and low-power circuits [3] are two potential uses for TI.

The features of TIs have piqued the interest of the scientific community due to experimental observations of surface states [4] in Bi_2Se_3 crystals and transport by edge states in HgTe quantum wells (QW) [5]. The edge states are either 2D states on the boundaries of 3D TI (as in the case of Bi_2Se_3 [6]) or 1D states on the boundaries of 2D TI (e.g., HgTe quamtum well). With the exception of HgTe [7], 2D and 3D TI samples are typically comprised of distinct compounds. Other realizations of 1D topologically protected states are found on step edges [8, 9] and on the edges between 3D TI surfaces [10].

The most striking feature of edge states in 2D TI is that, as a result of spin-momentum locking, the scattering event—which, in the case of a 2D TI edge, is always a back-scattering inevitably involves the quasiparticle's spin flipping. Consequently, the elastic scattering of the edge states is prohibited in the absence of magnetic impurities or other TR - violating contributions. This is the well-known manifestation of TR - symmetry in these kinds of systems [11]. Another important peculiarity of TI compounds is the pronounced spin-orbit interaction (SOI), [12, 13].

In paper [14], we introduced a model edge Hamiltonian describing the influence of SOI on edge imperfections. The edge imperfection is controlled by the deformation angle profile (see Fig. 1(a)). The elastic scattering becomes possible in the presence of the uniform magnetic field orthogonal to the edge. This model predicts an interesting effect. At not very strong magnetic fields the reflection coefficient exhibits pronounced oscillations as a function of magnetic field. In this paper we expand our study and discover new type of quantum oscillations of the reflection coefficient for another general type of potentials at Zeeman energies close to the energy of quasiparticles. We also extend the previous study on the deformation potential of yet another analytical structure. As usual, for the smooth deformation profiles the poweful Pokrovsky-Khalatnikov method [15] is used to obtain the analytic reflection amplitude with pre-exponential accuracy.

*Автор, ответственный за переписку: Ya. I. Rodionov, yaroslav.rodionov@gmail.com

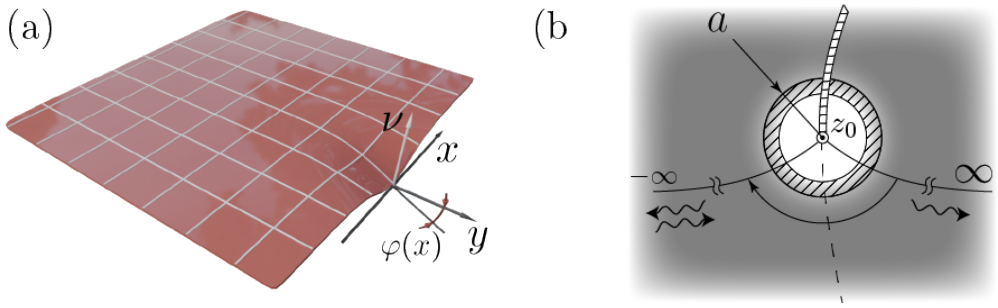

Рис. 1: A schematic illustration of a geometric imperfection on the edge of a 2D topological insulator sample

The paper is organized as follows. Section 1 is dedicated to the initial model and main approximations of the problem. Section 2 introduces the principle points of semiclassical Pokrovsky-Khalatnikov procedure. Section 3 deals with its application to the an important class of scattering potentials for slow moving edge excitations. Section 4 generalizes the previous treatment of the same problem to the wider class of potentials. Section 5 discusses the exact solution of the magnetic-field-free problem and presents the perturbation (in magnetic field) theory, as well as the matching of perturbative and semiclassical limit. We summarize the results in Section 6.

1 The model

The Hamiltonian of a 2D TI for the edge excitations has the following form [16]:

$$\hat{H} = H_0 + H_{so}, \quad H_0 = v_{F0}\hat{p}_x\hat{\sigma}_y, \quad H_{so} = \alpha\vec{\sigma}\times\vec{p}\cdot\vec{\nu}. \tag{1}$$

Here, H_0 is the effective Hamiltonian of edge states moving along x-axis (y=0) and $\vec{\sigma} = (\sigma_x, \sigma_y, \sigma_z)$ are Pauli matrices in the spin 1/2 basis and v_{F0} is a bare Fermi velocity.

The spin-orbital interaction Hamiltonian H_{so} is derived in paper [17] where a 2D electron gas was addressed; $\vec{p}$ is electron's momentum, ν is a unit normal to the surface of the TI (or to an interface in a heterostructure), and α is Rashba parameter. The latter depends on the external electric field (the gate voltage) [12,13] as well as the material. The former causes the splitting in energy bands due to electron's spin (Rashba splitting), which is pronounced in energy band structure of TI materials [13,18].

It is crucial to note here how the normal vector's ν direction should be fixed. Essentially, the right direction may be inferred from the original TI Hamiltonian, which we won't show here. Nevertheless, we rely on article [18], which demonstrates that a TI's Fermi velocity increases as Rashba's coefficient α decreases. The orientation shown in Fig. 1(a) corresponds to the correct direction of ν, as we will see below.

Let us consider a deformation at the edge, as depicted in Fig. 1(a). The tangent profile of the sample edge is bent in yz plane and determined by the function $\phi(x)$. This deformation leads to a transformed spin-orbit interaction

$$H_{so} = -\alpha\hat{p}_x\hat{\sigma}_y + \hat{U}(x), \quad \hat{U}(x) = \frac{\alpha}{2}[\hat{p}_x\phi(x) + \phi(x)\hat{p}_x]\sigma_z \tag{2}$$

for smooth and shallow defects ($\phi(x) \ll 1$). To preserve the hermicity of the initial SOI Hamiltonian (1) we introduced the anti commutator (due to the x-coordinate dependence of the normal vector ν). The first term in (2), $-\alpha\hat{p}_x\hat{\sigma}_y$ is a simple renormalization of the Fermi velocity, as we see from the initial Hamiltonian (1). The latter term in (2) is supposed to be treated as an elastic potential profile of the problem. In what follows, it would be convenient to incorporate the parameter α in the profile deformation function: $\varphi = \alpha\phi$.

The potential profile function $\hat{U}$ in (2) alone will not cause backscattering of the edge states, since $\hat{U}$ does not break TR - symmetry. However, that is not the case in the presence of the uniform magnetic field, since the latter does break the TR - symmetry. Therefore, we apply magnetic field in the vertical direction (z-axis) (i.e. orthogonal to the plane of the TI sample). The suitable gauge of vector-potential is as follows: $\vec{A} = (\mathcal{H}y, 0, 0)$. We note here, that y - coordinate remains constant in our case $y = \text{const}/$. Therefore, it can be safely put equal to zero (alternatively, for constant y the vector potential can be removed from Dirac's equation via elementary gauge transformation). Thus, the only change of the Hamiltonian brought by the magnetic field is the addition of a Zeeman term:

$$\hat{H}^{1D}(x) = v_F\hat{p}_x\sigma_y + \mu\sigma_z + \hat{U}(x). \tag{3}$$

Here, $v_F = v_{F0} - \alpha$ is a renormalized Fermi velocity and $\mu = \mu_B g \mathcal{H}$, g is the edge electron's g-factor [19]. We consider the application of the transverse magnetic field only. As shown in [20], the in-plane magnetic field can be eliminated by a gauge transformation of the electron field operators.

As a result, we end up solving the scattering problem for the following equation:

$$\left[v_F \hat{p}_x \sigma_y + \mu\sigma_z + \hat{U}(x)\right] \psi(x) = \varepsilon\psi(x) \tag{4}$$

As one readily sees, even in the absence of deformation potential $\hat{U}(x)$ the Zeeman term $\mu\sigma_z$ leads to a gap in the spectrum of edge state of the width μ. Therefore, the unbound states always obey the condition:

$$\varepsilon > \mu. \tag{5}$$

2 Methods

The Dirac equation (4) comprises two first order differential equations on the pair $\psi = (\psi_1,\ \psi_2)$. The most convenient approach to its analysis surprisingly happens to be the reduction of system (4) to a 2nd order differential equation on a single function ψ_1:

$$2\hbar^2\left(\varphi^2+1\right)\alpha\psi_1''+2i\hbar\left[\hbar^2\left(\varphi^2+1\right)\varphi''+\varphi\alpha\left(2\mu-3i\hbar\varphi'\right)\right]\psi_1' + \left[\frac{1}{2}\alpha\beta(\alpha - 2i\hbar\varphi') + 4\varepsilon\hbar^2\varphi\varphi''\right]\psi_1 = 0, \tag{6}$$

$$\psi_2 = \frac{2\hbar\left(\varphi^2+1\right)\psi_1' - i\psi_1\varphi\beta(x)}{\alpha(x)}. \tag{7}$$

Here $\alpha(x) = 2(\mu+\varepsilon) - i\hbar\varphi',\ \beta(x) = 2(\mu-\varepsilon) + i\hbar\varphi'$.

The derivation of (6) is straightforward and presented in [14]. Due to its complexity, differential equation (6) cannot be solved exactly. We are going to approach it from two different limits:
(i) semiclassical approximation, corresponding to the smooth deformation $\varphi(x)$ of the edge;
(ii) perturbation theory in magnetic field strength (Zeeman energy) μ. For the wide class of potentials we are going to show how these two approaches match.

2.1 Semiclassical approximation

First, we need to determine the small parameter of the problem. Physically speaking, semiclassical treatment corresponds to the case of smooth (on the scale of de Broglie wavelength) deformation potential $\varphi(x)$. The characteristic scale at which the potential changes is denoted as a_0. The smoothness of the potential then means:

$$\frac{\lambda}{a_0} \equiv \frac{\hbar v_F}{\varepsilon a_0} \ll 1 \quad (\textit{semiclassical approximation}) \tag{8}$$

The semiclassical scattering in the problem is structured in a way that, as we will see in the study that follows, the semiclassical momentum never vanishes on the real axis in view of condition (5), rendering the scattering an over-barrier event. Therefore, Pokrovsky-Khalatnikov [15] (P-Kh) method seems to be the most adequate approach to the task. For convenience, we use $\hbar = v_F = 1$ units system throughout the rest of the paper, restoring them when needed.

2.2 Pokrovsky-Khalatnikov approach

The concept of the method can be condensed to the following key steps (see also the work by M. Berry [21]):

(i) Perform the analytical continuation of the semiclassical solution into the complex plane along a so called anti-Stokes line, $\mathrm{Im}\int_{z_0}^{z} k(z)\,dz = 0$ where $k(z)$ is the semiclassical momentum and z_0 is the so called turning point in the complex plane.

(ii) Construct the exact solution of the Schrödinger equation around the turning point z_0, when the differential equation substantially simplifies due to the Taylor-expansion of momentum $k(z)$.

(iii) Determine the exact solution's asymptotics on the anti-Stokes lines that extend from the turning point to the left and right.

(iv) Presuming that there is a non-empty intersection of the range of existance of the asymptotics of exact and semiclassical solutions (the striped region in Fig. 1(b)) match the semiclassical and exact solutions in the mentioned range on anti-Stokes lines.

(v) Build an analytic continuation from the anti-Stokes line running to $-\infty$ on the real axis $\psi(z) \to \psi(x)$.

We are going to implement the outlined program step by step explaining all the nuances in the rest of the paper.

2.3 Semiclassical solution

Let us make the exponential substitute $\psi \to e^{iS/\hbar}$ for the wave function and employ the standard semiclassical expansion in the powers of $\hbar$ adapted to the equation (6):

$$\psi = \begin{pmatrix} \psi_1 \\ \psi_2 \end{pmatrix}, \quad \psi_{1,2} = \exp\left(\frac{iS_0}{\hbar} + iS_{1,2} + ...\right). \tag{9}$$

In the zeroth order in $\hbar$ (i.e. discarding all terms with derivatives of φ in Eq. 6) we obtain the following expression for S_0 [14]:

$$S_0(x) = \int^x q_\pm(x')\,dx', \tag{10}$$

$$q_\pm = \frac{-\mu\varphi \pm p}{\varphi^2+1}, \quad p = \sqrt{\varepsilon^2(\varphi^2+1) - \mu^2}, \tag{11}$$

where $q_\pm$ is interpreted as semiclassical momentum. The regular branch of p is chosen in such a way that $p \underset{x\to+\infty}{\to} \sqrt{\varepsilon^2-\mu^2}$. Then, retaining the next terms of order $\hbar$ ($S_{1,2}$ in the substitute (9)), and plugging it back in (6) we obtain the pre-exponential semiclassical terms for the wave function ψ:

$$\begin{aligned} &\psi_{1,\pm}(x) = \xi_{1,\pm}(x) e^{\frac{i}{\hbar}\int q_\pm\,dx} \quad \xi_{1,\pm} = \sqrt{\pm q_\pm\left[1 \pm \frac{\varphi\varepsilon}{p}\right]} \\ &\psi_{2,\pm}(x) = -i\psi_{1,\pm}\frac{\varepsilon\varphi \mp p}{\varepsilon+\mu}. \end{aligned} \tag{12}$$

The square roots entering the definition of $\xi_{1,\pm}$ are assumed to be positive at $x \to +\infty$. To clear out which of the solutions corresponds to the right (left) moving carriers we need semiclassical currents:

$$j_\pm \equiv \psi_\pm^\dagger \sigma_y \psi_\pm = \frac{2q_\pm}{p}(\varepsilon-\mu), \quad j_\pm \underset{x\to\infty}{=} \pm 2(\varepsilon-\mu). \tag{13}$$

In the last equation in (13) we take into account that deformation function $\varphi(x) \to 0$ at $x \to \pm\infty$

2.4 Transformation from Dirac to Schrödinger equation.

To make the analogy between Dirac equation Eq. 6 and Schrödinger equation explicit, we get rid of the first derivative in (6) via a standard substitute [22]. Therefore, the equation is transformed according to:

$$\begin{aligned} &\psi''(x) + \eta(x)\psi'(x) + \kappa(x)\psi(x) = 0 \Rightarrow \\ &\theta''(x) + \pi^2(x)\theta(x) = 0 \quad \text{(Schrödinger equation)} \end{aligned} \tag{14}$$

$$\theta(x) = e^{\frac{1}{2}\int^x \eta(t)dt}\psi(x), \tag{15}$$

$$\pi^2(x) = \kappa(x) - \frac{1}{2}\eta'(x) - \frac{1}{4}\eta^2(x). \tag{16}$$

The expression for $\pi^2(x)$ is quite cumbersome. Nevertheless, its is important, since it plays the role of the semiclassical momentum in the problem. Therefore, it is instructive to write down $\eta(x)$ and $\pi^2(x)$ discarding all the derivatives of the potential field $\varphi(x)$ (zeroth semiclassical approximation) as well as semiclassical solution. This way the connection with the initial semiclassical relations (10), (11) becomes transparent:

$$\eta(x) = \frac{2i}{\hbar}\frac{\mu\varphi(x)}{\varphi^2(x)+1}, \quad \pi^2(x) = \frac{\varepsilon^2(\varphi^2+1)-\mu^2}{(\varphi^2+1)^2} \tag{17}$$

$$\theta_\pm(x) = \frac{1}{\sqrt{\pi(x)}}\exp\left(\pm i\int_{x_0}^x \pi(t)dt\right). \tag{18}$$

In the last equation point x_0 needs to be chosen on the real axis. This way both functions $\theta_\pm$ have the same modulus. Apart from this x_0 is quite arbitrary and is picked from convenience considerations.

3 The reflection coefficient for the slow edge excitations

Now we would like to address quite a striking case of the over-barrier scattering in TI insulator. Suppose, the energy of the edge excitations is close to the Zeeman gap μ, so that the condition

$$|\varepsilon - \mu| \ll \varepsilon \tag{19}$$

is satisfied. It corresponds to the case of carriers with small momenta $v_F p \ll \mu$. This ought to be a realistic situation at temperatures much lower than Zeeman energy μ. As we are going to see, this situation also leads to a specific analytic structure of the momentum $\pi(z)$. Indeed, let us rewrite momentum $\pi(z)$, defined in Eq. 17 in a slightly different form:

$$\pi(z) = \frac{\varepsilon\sqrt{\varphi^2(z) + \frac{\varepsilon^2-\mu^2}{\varepsilon^2}}}{\varphi^2(z)+1}. \tag{20}$$

The last formula, in view of condition (19), shows that function $\pi(z)$ has two coalescent branch points positioned near the complex root of $\varphi(z_0) = 0$.

The semiclassical condition breaks down near these two coalescent branch points and we can employ step 2 from P-Kh method. We expand the semiclassical momentum near the point z_0, as follows:

$$\pi^2(z_0 + \zeta) = -\varepsilon^2\frac{\zeta^2}{a^2} + 2\delta\varepsilon\varepsilon, \tag{21}$$

where $\zeta = z - z_0$. Here, parameter a can be strictly speaking, complex. However, its modulus sets the characteristic scale of change of the potential. Therefore, one may assume that $|a| \sim a_0$, where a_0 is the scale of the deformation introduced in Eq. (8). This way, the Dirac equation (6) is turned into parabolic cylinder equation:

$$\psi_1'' - \varepsilon^2\left(\frac{\zeta^2}{a^2} - \frac{2\delta\varepsilon}{\varepsilon}\right)\psi_1(\zeta) = 0. \tag{22}$$

The anti-Stokes directions are given by the equation

$$\mathrm{Im}\int_0^\zeta \pi(t)\,dt \underset{\zeta\to\infty}{=} \varepsilon\mathrm{Re}\frac{\zeta^2}{2a} = 0 \;\Rightarrow\; \arg\zeta = \frac{\pi}{4} + \frac{\arg a}{2} + \pi n, \quad n \in \mathbb{Z}. \tag{23}$$

As a result, we choose the anti-Stokes lines with angles $-\pi/4 + \arg a/2$ and $-3\pi/4 + \arg a/2$. Substituting (21) into semiclassical expressions (10), (12) we obtain the semiclassical solution in the vicinity of point z_0

$$\begin{gathered}\psi_{<,+}(s) = \sqrt{2}\left[\frac{2s}{\gamma-1}\right]^{\frac{\gamma}{2}-1} e^{-\frac{is^2}{2}-\frac{i\pi\gamma}{8}-\frac{i\pi}{4}}[(\gamma-1)e]^{\frac{\gamma-1}{4}}, \quad \psi_{<,-}(s) = \sqrt{2}\left[\frac{2s}{\gamma-1}\right]^{-\frac{\gamma}{2}} e^{\frac{is^2}{2}+\frac{i\pi\gamma}{8}-\frac{i\pi}{2}}[(\gamma-1)e]^{-\frac{\gamma-1}{4}} \\ \psi_{>,+}(s) = \sqrt{2}\left[\frac{2s}{\gamma-1}\right]^{\frac{\gamma}{2}-1} e^{\frac{is^2}{2}+\frac{i\pi\gamma}{8}-\frac{i\pi}{2}-\frac{\gamma-1}{4}}[(\gamma-1)e]^{\frac{\gamma-1}{4}}\end{gathered} \tag{24}$$

Now, to proceed further we need to find exact solutions of Eq. (22)

3.1 Exact solution at the double branch point. Match with semiclassical wave functions.

Introducing variable change: $\zeta = \sqrt{a/\varepsilon}se^{-i\pi/4}$, we obtain the differential equation

$$\psi_1'' + (s^2 - 2i\delta\varepsilon a/\varepsilon)\psi_1 = 0. \tag{25}$$

The standard change: $\psi_1(s) = e^{-is^2/2}\chi$ turns it into an equation with linear coefficients:

$$\chi'' - 2is\chi' - i\gamma\chi, \quad \gamma = 1 + 2\varepsilon a\frac{\delta\varepsilon}{\varepsilon}. \tag{26}$$

Laplace procedure yields:

$$\chi(s) = A\int_C e^{st+it^2/4}t^{\gamma/2-1}\,dt, \quad A = \frac{1}{\sqrt{2\pi}}e^{-\frac{i\pi}{8}(\gamma-1)}\left(\frac{\varepsilon}{a}\right)^{1/4}\frac{e^{\frac{\gamma-1}{4}}}{(\gamma-1)^{\frac{\gamma}{4}-\frac{3}{4}}}, \tag{27}$$

where contour C is chosen in such a way that function $V = e^{st+it^2/4}t^{\gamma/2}$ assumes identical values on its end points. The choice of the contour and the branch cut is dictated by the asymptotic behavior. Using saddle point approximation we obtain for the asymtptics on the right anti-Stokes line:

$$\chi(s)\Big|_{\arg\zeta=-i\pi/4} = \sqrt{4\pi}(2s)^{\frac{\gamma}{2}-1}e^{-\frac{is^2}{2}+\frac{i\pi}{4}}, \quad \chi(s)\Big|_{\arg\zeta=-3\pi i/4} = e^{-\frac{is^2}{2}+\frac{i\pi}{4}} - 2i\sin\frac{\pi\gamma}{2}e^{\frac{i\pi\gamma}{4}}\frac{\Gamma\left(\frac{\gamma}{2}\right)}{s^{\gamma/2}}e^{is^2/2}. \quad (28)$$

Matching exact solutions with semiclassical solutions (24) we obtain:

$$\psi_<(s) = e^{\frac{i\pi}{8}}\left(i\psi_{<,+} + 2\sin\frac{\pi\gamma}{2}\frac{\Gamma\left(\frac{\gamma}{2}\right)}{\sqrt{2\pi}}\left[\frac{\gamma-1}{2e}\right]^{\frac{\gamma-1}{2}}\psi_{<,-}\right). \quad (29)$$

which gives us the reflection coefficient in the form

$$R = \frac{2}{\pi}\left|\cos^2\left(\frac{\pi a\delta\varepsilon}{\hbar v_F}\right)\Gamma\left(\frac{1}{2}+\frac{a\delta\varepsilon}{v_F\hbar}\right)\right|^2\left|\frac{a\delta\varepsilon}{e\hbar v_F}\right|^{\frac{2a\delta\varepsilon}{\hbar v_F}}\exp\left(-\frac{4}{\hbar}\mathrm{Im}\int_{x_0}^{z_0}\frac{\sqrt{\varepsilon^2(\varphi^2+1)-\mu^2}}{\varphi^2+1}\,dz\right), \quad (30)$$

where we restored v_F and Planck's constant $\hbar$ from dimensional considerations. Here, point x_0 as was mentioend before, should be chosen somewhere on the real axis (a particular choice of x_0 doesn't affect the imaginary part of the integral). Eq. (30) is one of the main results of the paper. Due to the presence of the pre-exponential factor, the reflection coefficient R reveals quantum oscillations as a function of the energy of the incident particle ε for general type of analytic potentials. It is important to stress, that result (30) cannot be continued to the case of small or vanishing magnetic fields $\mu \to 0$, since $\delta\varepsilon \equiv \varepsilon - \mu \ll \varepsilon$ and $\varepsilon \gg \frac{\hbar v_F}{a}$.

4 Potential with a second-order pole

In this part of the paper we would like to expand the treatment in paper [14] on the case of a yet another type of deformation profile. In paper [14] only the potentials with the first order pole in the complex plane were considered. These are the so-called Lorentzian-type potentials. Now we would like to expand this treatment and consider the case of the potential which has the second-order pole on the complex plane. Eventually, our method paves the way for the treatment of the potential possessing the pole of any order in the complex plane. However, as the order of the pole gets higher, the respective analytic expressions become quite cumbersome. Therefore, we restrict our attention to the doable case of the second order pole. As in [14] we perform the Laurent expansion near the pole:

$$\varphi(z) = \frac{ia^2}{(z-z_p)^2} + \ldots \quad (31)$$

As before, the complex parameter a sets the scale of the deformation profile: $|a| \sim a_0$. Next, according to step 2 of the P-Kh method, we proceed with the semiclassical study of the respective Dirac equation in the vicinity of the pole z_p.

4.1 The semiclassical solution in the vicinity of the pole

The equation for anti-Stokes lines is easily obtained in the vicinity of point z_p along the lines outlined in step 2 of P-Kh procedure. With the help of potential expansion (31) we obtain:

$$\mathrm{Im}\int_0^\zeta \pi(t)\,dt = \mathrm{Im}\left[-\frac{i\varepsilon}{a^2}\int_0^\zeta t^2 dt\right] = -\frac{\varepsilon\mathrm{Re}\,\zeta^3}{3a^2} = 0 \;\Rightarrow\; \arg\zeta = \frac{2\arg a}{3} - \frac{\pi}{6} + \frac{\pi n}{3}, \quad n\in\mathbb{Z}. \quad (32)$$

Here, as before $\zeta \equiv z - z_p$. We see that anti-Stokes lines form $\pi/6$ directions (up to the rotation by $\arg a$) with the real axis. Finally, we are ready to write down the semiclassical solutions:

$$\psi_{1+,\gtrless} = \frac{\varepsilon+\mu}{\varepsilon}\frac{\zeta^3}{a^3}\sqrt{\varepsilon-\mu}e^{-\frac{\varepsilon+\mu}{3a^2}\zeta^3+\frac{3\pi i}{4}} \quad \psi_{1-,<} = \sqrt{2(\varepsilon-\mu)}\frac{\zeta}{a}e^{\frac{i(\varepsilon-\mu)}{3a^2}\zeta^3+\frac{i\pi}{4}} \quad (33)$$

4.2 The exact solution in the vicinity of the pole. Match with semiclassical solutions.

The principal and most nontrivial part of the solution is to obtain the exact solution near the pole. The differential equation in the vicinity of the pole has a quite terrifying appearance. However, due to the presence of initial external initial TR -symmetry, the educated substitutes drastically simplify it. The semiclassical

solution of the differential equation looks as follows: $\psi_s(\zeta) = \zeta \exp[(\varepsilon-\mu)\zeta^3/(3a^2)]$. As a result, the substitute $\psi_1(\zeta) = \psi_s(\zeta)\psi(\zeta)$ leads to a much simpler equation

$$a^2\zeta\psi''(\zeta)\left[a^2-\zeta^3(\mu+\epsilon)\right] - \psi'(\zeta)\left[a^4 - 2a^2\zeta^3(2\mu+3\epsilon) + 2\zeta^6\epsilon(\mu+\epsilon)\right] = 0. \tag{34}$$

Eq. (34) is integrated in quadratures:

$$\psi_1(\zeta) = \zeta e^{\frac{\zeta^3(\epsilon-\mu)}{3a^2}}\left[c_1\left\{2\Gamma\left(\frac{2}{3},\frac{2\zeta^3\epsilon}{3a^2}\right) - 3\left(\frac{\mu}{\epsilon}+1\right)\Gamma\left(\frac{5}{3},\frac{2\zeta^3\epsilon}{3a^2}\right)\right\} + c_2\right], \tag{35}$$

where $\Gamma(a,z) = \int_z^\infty t^{a-1}e^{-t}\,dt$ is the incomplete Γ - function.

Now we need to find the asymptotics and match it with semiclassical solutions. The asymptotics read:

$$\psi_1(\zeta) \underset{\zeta\to+\infty}{=} c_2\zeta e^{\frac{\zeta^3(\epsilon-\mu)}{3a^2}} - \frac{2^{2/3}\sqrt[3]{3}c_1\left(\zeta^3\epsilon(\mu+\epsilon)\right)e^{-\frac{\zeta^3(\mu+\epsilon)}{3a^2}}}{(a\epsilon)^{4/3}} \tag{36}$$

To the right of the pole we have the transmitted wave only, hence:

$$c_2 = 0, \quad c_1 = -e^{3\pi i/4}\frac{1}{\varepsilon^{2/3}a^{5/3}}\sqrt{\frac{\varepsilon-\mu}{2}}\frac{1}{2^{2/3}3^{1/3}}. \tag{37}$$

Once we switch from the anti-Stokes line $\zeta \to |\zeta|e^{-i\pi/6}$ (transmitted wave) to the anti-Stokes line $\zeta \to |\zeta|e^{-5i\pi/6}$ (incident wave) we analytically continue $\Gamma(a,z)$. We see that the argument: $2\zeta^3\varepsilon/(3a^2)$ rotates by -2π as ζ changes from $-\pi/6 + (2/3)\arg a$ to $-5\pi/6 + (2/3)\arg a$ and the corresponding change in the asymptotics of the incomplete Γ - function:

$$\Gamma\left(a, ye^{-5\pi i/2}\right) = e^{-5\pi i/2}y^{a-1}ie^{iy} + \Gamma(a)e^{-\pi i a}2i\sin\pi a. \tag{38}$$

This way, we find the following asymptotics of the solution:

$$\psi(\zeta) = c_1\left[2e^{i\pi/3}\frac{\sqrt{3i}\mu}{\varepsilon}\Gamma\left(\frac{2}{3}\right)ze^{\frac{\varepsilon-\mu}{3a^2}z^3} - \frac{2^{2/3}3^{1/3}(\varepsilon+\mu)z^3}{a^{4/3}\varepsilon^{1/3}}e^{-\frac{\varepsilon+\mu}{3a^2}z^3}\right] \tag{39}$$

Next, the solution can be matched with the semiclassical waves to get:

$$\psi_1(\zeta)\Big|_{\text{left}} = \psi_{1+,<}(\zeta) + e^{i\pi/3}\frac{\mu}{\varepsilon}\frac{3^{1/6}}{2^{2/3}}\frac{\Gamma\left(\frac{2}{3}\right)}{(a\varepsilon)^{2/3}}\psi_{1-,<}(\zeta). \tag{40}$$

As a result, we match the solution with the semiclassical waves (33) to obtain the reflection coefficient:

$$R = \frac{\mu^2}{\varepsilon^2}\frac{3^{1/3}}{2^{4/3}}\frac{\Gamma^2\left(\frac{2}{3}\right)}{(a\varepsilon)^{4/3}}\exp\left(-\frac{4}{\hbar}\mathrm{Im}\int_{x_0}^{z_0}\frac{\sqrt{\varepsilon^2(\varphi^2+1)-\mu^2}}{\varphi^2+1}\,dz\right) \tag{41}$$

Eq. (41) complements result (30) for the case of not very slow edge excitations: $\varepsilon \sim \mu$. However, the value of result (41) lies in the fact, that it can be continued to the case of a zero magnetic field, where, according to TR-symmetry the reflection coefficient must strictly vanish. And indeed, we see, that at $R \underset{\mu\to0}{\to} 0$. To check the consistency of the result we complement our study with the perturbation theory in μ in what follows. Our goal is to match result (41) with the perturbative calculation for the case of smooth deformation.

5 Perturbation theory in μ.

We need to analyze the scattering problem in the weak magnetic field limit $\mu \ll \varepsilon$, restricting ourselves to the first Born approximation. TR-symmetry of the problem gives us a nice present here. Surprisingly, we have found an exact solution of the Dirac equation (4) in the absence of the magnetic field $\mu = 0$ for any deformation potential [14]. Expectedly, due to TR-symmetry, the exact solution is reflectionless. Now we are going to see, how even the slightest magnetic field affects the analytical structure of the solution and leads to non-zero reflection in the problem.

5.1 Exact solution

Let us rewrite the initial Hamiltonian in the absence of magnetic field:

$$H = v_F \sigma_y \hat{p} + \frac{\sigma_z}{2}(\varphi\hat{p} + \hat{p}\varphi) \tag{42}$$

It happens one can contrive a unitary transformation

$$\psi(x) = \hat{U}(x)\tilde{\psi}(x), \quad \hat{U}(x) = \exp[i\theta(x)\sigma_x], \quad \tan 2\theta(x) = \varphi^{-1}(x),, \tag{43}$$

turning Hamiltonian (42) to much simpler form [14]:

$$\tilde{H} = \frac{1}{2}(v\hat{p} + \hat{p}v)\sigma_z, \tag{44}$$

where $v(x) = v_F\sqrt{\varphi^2(x)+1}$. Hamiltonian (44) has the following exact eigenfunctions (see the derivation in [14]):

$$\underset{\rightarrow}{\psi_\varepsilon}(x) = \frac{e^{i\varepsilon\tau(x)}}{\sqrt{v(x)}}\begin{pmatrix}1\\0\end{pmatrix}, \quad \underset{\leftarrow}{\psi_\varepsilon}(x) = \frac{e^{-i\varepsilon\tau(x)}}{\sqrt{v(x)}}\begin{pmatrix}0\\1\end{pmatrix}, \tag{45}$$

$$\tau(x) = \int\limits_0^x \frac{dx'}{v(x')} \equiv \int\limits_0^x \frac{dx'}{\sqrt{\varphi^2(x')+1}}. \tag{46}$$

And one clearly sees that the forward moving exact solution in (45) remains such in the entire real axis and we have the reflectionless situation expected from the TR symmetry of the system.

5.2 Perturbation theory in μ.

To build the perturbation theory, we need the Green's function for the transformed Hamiltonian (44) [14]:

$$G(\epsilon; x, x') = -\frac{i}{2}(1 + \mathrm{sign}[\tau(x) - \tau(x')]\sigma_z)\frac{e^{i\epsilon|\tau(x)-\tau(x')|}}{\sqrt{v(x)v(x')}}, \tag{47}$$

where $\mathrm{sign}\,(x)$ is a sign function. Then we consider the perturbation created by magnetic field; in the initial basis it is $V = \mu\sigma_z$. Under the unitary transformation $\hat{U}$ it becomes:

$$\tilde{V}(x) = \frac{\mu}{\varphi^2(x)+1}\left[\varphi(x)\sigma_z - \sigma_y\right]. \tag{48}$$

Then, the reflected wave is given by the perturbation theory:

$$\psi_{\mathrm{ref}}(x) = -\int\limits_{-\infty}^{\infty} G(\epsilon; x, x')\tilde{V}(x')\underset{\rightarrow}{\psi_\varepsilon}(x')\,dx'. \tag{49}$$

Plugging the transformed scattering potential (48), the Green's function (47) into (49), we obtain (after some simple algebra) the reflected wave in the first order perturbation theory:

$$\psi_{\mathrm{ref}} = r\underset{\leftarrow}{\psi_\varepsilon}(x), \quad r = \mu\int\limits_{-\infty}^{\infty}\frac{e^{2i\varepsilon\tau(x')}}{1+\varphi^2(x')}dx', \tag{50}$$

where r is the final reflection amplitude in Born approximation. A shrewd reader is going to immediately notice that the integral defining r is divergent. It can be easily argued that, one should understand this integral as a taken along the inclined directions $-\infty \to \infty e^{i\pi-\delta}$ and $\infty \to \infty e^{i\delta}$ where δ is an arbitrarily small positive angle.

Now we need to match the perturbative result (50) with the semiclassical relation (41). To this end we perform integration in the integral entering (50) in the saddle point approximation. Indeed, the semiclassical case corresponds to the large parameter $\varepsilon\tau(x)$ in the exponent of the integrand in (50). The saddle point analysis of the integral in question pleasantly resembles the semiclassical treatment undertaken in the previous section. The saddle of the $\tau(z)$ is the pole of the function $\varphi(z)$. Since the pole of the second order, so is the saddle.

$$\tau(z_p + \zeta) = \tau(z_p) + \int_{z_p}^{z_p+\zeta}\frac{dt}{\sqrt{\varphi^2(t)+1}} = \tau(z_p) + \frac{\zeta^3}{3ia^2} + \ldots \tag{51}$$

We have thee steepest descent lines sprawling from the saddle at directions $\varphi = \pi/3 + (2/3)\arg a + 2\pi n/3$. Choosing the direction $n = -1$ and $n = 1$ we obtain the two Γ-function-type integrals. As a result, the saddle point approximation yields:

$$\int\limits_{-\infty}^{\infty} \frac{e^{2i\varepsilon\tau(x')}}{1+\varphi^2(x')}dx' = -\frac{1}{a^4}\frac{\Gamma\left(\frac{2}{3}\right)}{3}\left(\frac{3}{2}\right)^{2/3}\left(\frac{a^2}{\varepsilon}\right)^{5/3} e^{-i\pi/3}\exp\left[2i\varepsilon\tau(z_p)\right]. \tag{52}$$

which up to a phase coincides with the reflection amplitude in (40). As a result, the reflection coefficient presented by perturbation theory (50) coincides exactly for the case of smooth potential with the weak field limit $\mu \ll \varepsilon$ of the semiclassical expression (41) which presents a pleasant twofold corroboration of our study.

Reflection coefficients (30) and (41) are the main results of our paper. The former predict the emergence of quantum oscillations of the 1D Landauer conductance of the slow edge excitations at uniform external magnetic field for the deformation profile of a general type.

6 Discussion

To conclude, we studied analytically the scattering of the quasiparticles on edge imperfections of 2D TI in the uniform magnetic field. We used two mutually complementing approaches: Pokrovsky-Khalatnikov method and perturbation theory in magnetic field. We obtained the reflection coefficients for two important physical situations and made sure the results obtained match in the shared domain of validity of both treatments. The study reveals the nontrivial interconnection between TR symmetry and the analytical properties of the reflection amplitude.

Our results may also be checked experimentally. The perturbation theory results are obviously valid for sufficiently small external magnetic field. The semiclassical parameter $\lambda/a_0 = \hbar v_F/(\varepsilon a_0)$ is easy to estimate from typical experimental data. For 2D TI formed in gated HgTe quantum well, the Rahsba splitting parameter $\alpha \sim 10$ eVÅ, [23], the Fermi velocity $v_F \approx 2$ eVÅ, [24]. We see that Rashba parameter α is approximately of the same order as Fermi velocity $\alpha \sim v_R$. Therefore, for the typical experiment, the 1μm size edge defect exceeds by far the quasiparticle wave length $\lambda \sim 100$Å, [25] which justifies the use of semiclassical approximation. Next, we would like to estimate the magnetic field at which the quantum oscillations predicted by the expression for the reflection coefficient (30) can be observed. The g - factor for helical edge states under the transverse magnetic field was measured in [26]: $g \approx 50$. Therefore, assuming the typical deformation scale as ~ 1 μm, the needed magnetic field is $H \sim v_F\hbar/(g\mu_B a_0) \sim 0.07$ T.

Список литературы

[1] Nayak C., Simon S. H.,Stern A.,Freedman M., and Das Sarma S. Non-Abelian anyons and topological quantum computation // Rev. Mod. Phys. — 2008. — Sep. — Vol. 80, issue. 3— P. 1083–1159. —

[2] Moore J. The next generation // Nature Physics — 2009. — Jun. — Vol. 5, no. 6— P. 378–380. —

[3] I. Žutíc, J. Fabian, and S. Das Sarma Spintronics: Fundamentals and applications // Rev. Mod. Phys. — 2004. — Apr. — Vol. 76. — P. 323–410. —

[4] Hsieh D., Qian D., Wray L., Xia Y., Hor Y. S., Cava R. J. and Hasan M. Z. A topological Dirac insulator in a quantum spin Hall phase // Nature Physics — 2008. — Apr. — Vol. 452, no. 7190— P. 970–974. —

[5] König M., Wiedmann S., Brüne C., Roth A., Buhmann H., Molenkamp L. W., Qi X.-L., and Zhang S.-C. Quantum Spin Hall Insulator State in HgTe Quantum Wells // Science — 2007. — Nov. — Vol. 318, no. 5851— P. 766–770. —

[6] Zhang H., Liu C.-X. Qi, Dai X., Fang Z., Zhang S.- C. Topological insulators in Bi2Se3, Bi2Te3 and Sb2Te3 with a single Dirac cone on the surface // Nature Physics — 2009. — May. — Vol. 5, no. 6— P. 438–442. —

[7] Kvon Z. D.,Kozlov D. A., Olshanetsky E. B., Gusev G. M.,Mikhailov N. N., and Dvoretsky S. A. Topological insulators based on HgTe // UFN — 2020. — Jul. — Vol. 63, no. 7— P. 629–647. —

[8] Herath T. M.,Hewageegana P., Apalkov V. Electron scattering by a steplike defect in topological insulator nanofilms // Physical Review B — 2013. — Feb. — Vol. 87, no. 7— P. 075318. —

[9] Fedotov N. I., Zaitsev-Zotov S. V. Experimental search for one-dimensional edge states at surface steps of the topological insulator: Distinguishing between effects and artifacts // Physical Review B — 2017. — Apr. — Vol. 95, no. 15— P. 075318. —

[10] Deb O., Soori A., Sen D., Edge states of a three-dimensional topological insulator // Journal of Physics: Condensed Matter — 2014. — Jul. — Vol. 26, no. 31— P. 315009. —

[11] Kane C. L. and Mele E. J. Quantum Spin Hall Effect in Graphene // Phys. Rev. Lett. — 2005. — Nov. — Vol. 95, no. 22— P. 226801. —

[12] Hinz J., Buhmann H., Sch¨afer M., Hock V., Becker C. R., Molenkamp L. W. Gate control of the giant Rashba effect in HgTe quantum wells // Semiconductor Science and Technology — 2006. — Mar. — Vol. 21, no. 4— P. 501–506. —

[13] Yang Hong, Peng Xiangyang, Liu Wenliang, Wei Xiaolin, Hao Guolin, He Chaoyu, Li Jin, Stocks G Malcolm, Zhong Jianxin Electric tuning of the surface and quantum well states in Bi_2Se_3 films: a first-principles study // Journal of Physics: Condensed Matter— 2014. — aug. — Vol. 26— P. 395005. —

[14] Dotdaev A. S., Rodionov Ya. I., Rozhkov A. V., Grigoriev P. D. Semiclassical scattering by edge imperfections in topological insulators under magnetic field // arxiv — 2024. — Aug. — arXiv:2408.14540—

[15] Pokrovskii VL, Khalatnikov IM On the problem of above-barrier reflection of high-energy particles // Soviet Phys. JETP— 1961. — Vol. 13— P. 1207–1210. —

[16] Qi Xiao-Liang, Zhang Shou-Cheng Topological insulators and superconductors // Rev. Mod. Phys.— 2011. — Oct. — Vol. 83, no. 4— P. 1057–1110. —

[17] Bychkov Yu A, Rashba E I Oscillatory effects and the magnetic susceptibility of carriers in inversion layers // Journal of Physics C: Solid State Physics— 1984. — nov. — Vol. 17— P. 6039–6045. —

[18] Zhang Yi, He Ke, Chang Cui-Zu, Song Can-Li, Wang Li-Li, Chen Xi, Jia Jin-Feng, Fang Zhong, Dai Xi, Shan Wen-Yu, Shen Shun-Qing, Niu Qian, Qi Xiao-Liang, Zhang Shou-Cheng, Ma Xu-Cun, Xue Qi-Kun Crossover of the three-dimensional topological insulator Bi2Se3 to the two-dimensional limit // Nature Physics— 2010. — jun. — Vol. 6— P. 584–588. —

[19] Kernreiter Thomas, Governale M., Zuelicke Ulrich, Hankiewicz Ewelina Anomalous Spin Response and Virtual-Carrier-Mediated Magnetism in a Topological Insulator // Physical Review X— 2016. — 04. — Vol. 6— P. 021010. —

[20] Zyuzin A. A., Hook M. D., Burkov A. A. Parallel magnetic field driven quantum phase transition in a thin topological insulator film // Phys. Rev. B— 2011. — Jun. — Vol. 83, no. 24— P. 245428. —

[21] Berry Michael V Semiclassically weak reflections above analytic and non-analytic potential barriers // Journal of Physics A: Mathematical and General— 1982. — Vol. 15— P. 3693. —

[22] E. T. Whittaker and G. N. Watson, A course of modern analysis: an introduction to the general theory of infinite processes and of analytic functions; with an account of the principal transcendental functions (University press, 1920).

[23] Schultz M, Heinrichs F, Merkt U, Colin T, Skauli T, Løvold S Rashba spin splitting in a gated HgTe quantum well // Semiconductor science and technology— 1996. — Vol. 11— P. 1168. —

[24] Krishtopenko S. S., Teppe F. Realistic picture of helical edge states in HgTe quantum wells // Phys. Rev. B— 2018. — Apr. — Vol. 97, no. 16— P. 165408. —

[25] Dantscher K-M, Kozlov DA, Scherr MT, Gebert Sebastian, Bärenfänger Jan, Durnev MV, Tarasenko SA, Bel'Kov VV, Mikhailov NN, Dvoretsky SA, others Photogalvanic probing of helical edge channels in two-dimensional HgTe topological insulators // Physical Review B— 2017. — Vol. 95— P. 201103. —

[26] Yakunin M.V., Podgornykh S.M., Mikhailov N.N., Dvoretsky S.A. Spin splittings in the n-HgTe/CdxHg1-xTe(013) quantum well with inverted band structure // Physica E: Low-dimensional Systems and Nanostructures— 2010. — Vol. 42— P. 948-951. —

РАССЕЯНИЕ НА ДЕФОРМИРОВАННОМ КРАЕ В ТОПОЛОГИЧЕСКИХ ИЗОЛЯТОРАХ В ОДНОРОДНОМ МАГНИТНОМ ПОЛЕ

Родионов Я.И.[1*]

[1] Институт теоретической и прикладной электродинамики, Москва, 125412, Россия
[*] yaroslav.rodionov@gmail.com

Аннотация

Исследуется рассеяние краевых возбуждений на краевых дефектах двумерного топологического изолятора (ТИ) в однородной внешнем магнитное поле. Кравевые дефекты повсеместно встречаются в реалистичных 2D ТИ. Наши предыдущие исследования показывают возможность существования колебаний амплитуды отражения в слабом магнитном поле. В этой статье мы рассматриваем еще один общий класс профилей краевой деформации, а также предсказываем новые квантовые осцилляции коэффициента рассеяния в еще одной общей ситуации носителей малого импульса. Для получения коэффициента отражения с предэкспоненциальной точностью используется квазиклассический подход Покровского-Халатникова.

Ключевые слова: Топологические изоляторы, квазиклассическое рассеяние

УДК 535.375.5

PLASMON ZEBRA RESONANCES AND NANOPAINTING

A.K. Sarychev * [1], A.V. Ivanov[1], D.J. Bergman[2], R. Fan[3], A.F. Smyk[4]

[1] *Institute for Theoretical and Applied Electrodynamics, Russian Academy of Sciences, Moscow, Russia*
[2] *Tel Aviv university, Tel Aviv University, Tel Aviv, Israel*
[3] *Shanghai Maritime University, Shanghai, China*
[4] *James River Branch llc, Moscow, Russia*

Received: 23.09.2024
Accepted: 06.11.2024
Published: 19.11.2024

Abstract

We investigate metal-dielectric metasurfaces composed from periodic metal nanostrips deposited on a dielectric substrate. The metasurface can be termed as plasmon zebra (PZ). The metasurface operates as a set of open plasmon resonators. The theory of plasmon, excited in the open, interconnect resonators, is developed. The large local electromagnetic field is predicted for optical frequencies when plasmon is exited. The reflectance of PZ is much enhanced at the frequency of plasmon resonance and PZ ascribe the color corresponding to the resonance frequency. We propose PZ as simplest but easy tuning plasmon painting.

Keywords: plasmon resonance, nanopaint, SERS

EDN VAUPVG

doi:10.24412/2949-0553-2024-513-25-36

1. Introduction

Optical surface waves, known as surface plasmons (SP), can get excited in metal films. The metal permittivity $\varepsilon_m = \varepsilon'_m + \varepsilon''_m$ is mainly negative for good optical metals like silver or gold where $\varepsilon'_m < 0$ and $\varepsilon''_m \ll |\varepsilon_m|$. SP, which is electromagnetic field bounded with electric charges, can propagate in the metal nanofilms that thickness $2h$ is much less than the wavelength λ. For example, the symmetric SP, where surface charges have the same signs on both film sides, propagates in a metal nanofilm. The wavevector q of the symmetric SP is proportional to $q \sim -\varepsilon_d/(\varepsilon_m h)$, recall that $\varepsilon'_m < 0$. The esteem is obtained for the thin film ($d \ll \lambda$) by considering the film as an inductive plane. Mean free-path estimates as $l_p = 1/\Im q \sim h\,|\varepsilon_m|^2/(\varepsilon_d \varepsilon''_m) \gg h$, so that it is much larger than the film thickness. The incident light cannot excite SP in the unbound, infinite metal plane since SP velocity is always less than the speed of light. Yet, SP can be easily excited in any finite peace of the of the metal film since SP transfers momentum to the environment by reflecting from the edges. The propagating SP reflects from the edges of the metal film and forms a standing wave. That is a finite patch of the metal film operates as an open plasmon resonator in optical and infrared frequency bands. For example, the simple system of the parallel metal strips operates as a set of the interconnecting plasmon resonators. This plasmon zebra (PZ) system is shown in Fig. 1. SP being excited in x direction, which is perpendicular to the PZ strips, reflects from edges of a strip. It can also jump from one strip to the neighboring strips. That is SP propagates in the transversal direction (x direction in Fig. 1). The phase speed of the transversal SP depends on the PZ parameters. Therefore its wavevector q can be fitted to an arbitrary value by varying the width, thickness of the metal strips as well as by change the gap between strips. The reflectance has maximum(s) at the resonance(s). Being illuminate by natural light PZ ascribe the color in reflection corresponding to the frequency of the plasmon resonance.

To simplify the consideration the quasistatic approximation is used that conveys the main features of the plasmon resonance. We assume that the PZ period is less than $\lambda/2$. Then the incident light does not diffract at the PZ but just produces reflected and transmitted EM waves. The evanescent waves, localized around the subwavelength PZ, are mainly due to excitation SP in the PZ. EM properties can be discussed in terms of the effective permittivity ε_e, i.e., the film conductance Σ_e, and effective permeability μ_e. Note

*Автор, ответственный за переписку: Сарычев Андрей Карлович, sarychev_andrey@yahoo.com

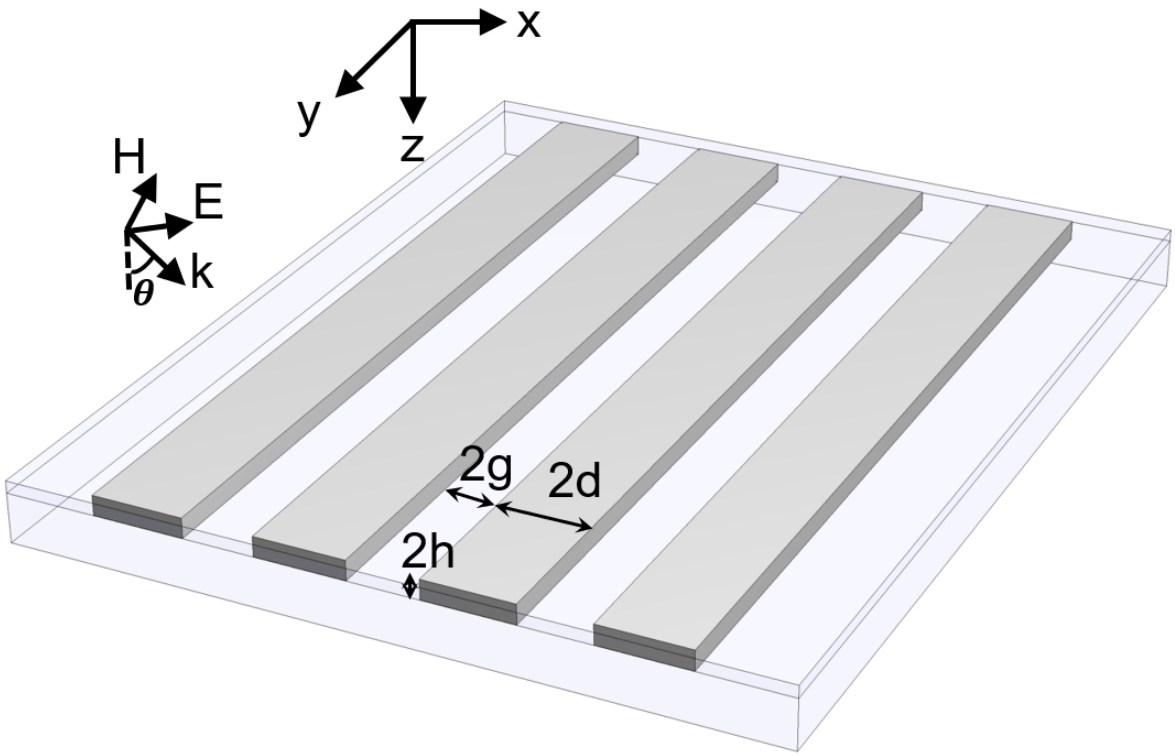

Рис. 1: Metal plasmon zebra (PZ) composed from parallel metal strips (gray color) with thickness $2h$ and width $2d$ that are separated by interstrip gates with width $2g$; period of PZ equals to $2(d+g)$. Light is incident from above at angle θ to the normal. The metal strips are staffed between substrate with permittivity ε_d and upper dielectric protective layer with permittivity ε_e.

the permeability μ_e almost equal to one for the thin PZ. Optical reflectance from PZ achieves maximum when SP is excited in PZ strips. The natural light is composed from EM waves of various wavelengths. The light reflected from PZ is composed mainly from the wavelengths corresponding to the SP resonances. That is metal subwavelength PZ has a color that depends, in general, on the angle of the incidence and light polarization. By fitting the parameters of PZ can be used as a plasmon painting with any wanted color and almost zero thickness. The glass coloring by plasmon nanoparticles was known from the time of the ancient Egypt (see, e.g., Lycurgus Cup in the British museum [1]). One can see the plasmon paintings does not fade for many centuries. Plasmon structures are considered as main ingredient responsible for the beautiful European cathedral-stained glass windows [2]. Recent nanotechnology pave the way for mass production of the light, flexible, nanothin and almost eternal plasmon paintings. Moreover, plasmon paintings are environmentally friendly since they do not contains dies, which are very often rather toxic [3]. Various technologies were studied [4–6] including electron beam lithography [7–15] ion milling, [8, 16–18] and nanoimprint lithography [7]. In recent work of Shalaev's group [19] a sustainable, lithography-free process is demonstrated for generating non fading plasmon colors with a prototype device that produces a wide range of vivid colors. The extended color palette is obtained through photo-modification by the heating of the localized SP under femtosecond laser illumination [20]. The proposed printing approach can be extended to other applications including laser marking, anti-counterfeiting, and chrome-encryption.

In this paper we present analytical theory for propagating or localized SP in PZ, which is the simplest possible periodic plasmon metasurface consisting of the parallel metal nanostrips. The explicit equations are derived for the reflectance as well as for the local EM field. We use the GOL approximation [21,22] considering EM field around PZ in self consistent way. SP propagating in the lateral directions along the metasurface are incorporated in GOL approach. The developed theory gives the value of the resonance local electric field that can be enhanced by orders on magnitude compared to the impinged light. The reflectance, local field and SERS were found in the system of silicone bars covered by the silver film shown in Fig. 2 [23–26]. Since the resonance fields are much enhanced in the silver bars of this PZ, it is used as SERS substrate. The smooth spatial structure of the film is convenient for the analyte deposition and can be tuned for effective adsorbing and sensing microscopic objects like protein molecules or viruses [27–29].

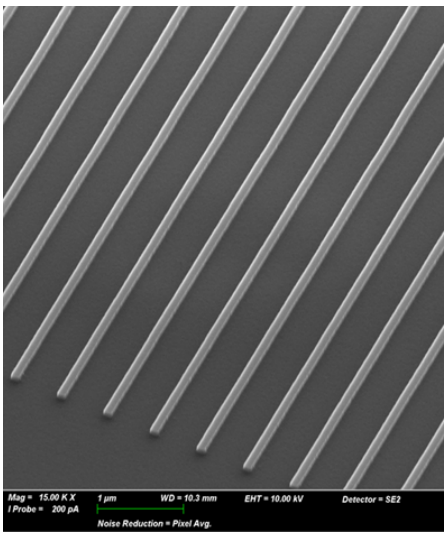

Рис. 2: Scanning electron microscopy image of the silver zebra on silicone substrate (reprint from [24]).

2. Quasistatic Theory of Plasmon Resonance

We consider the interaction of a nanothin-thin metal film with thickness $2h$ with an incident light. As it was mentioned above the metal permittivity $\varepsilon_m = \varepsilon'_m + \varepsilon''_m$ is mainly negative, namely, $\varepsilon'_m < 0$ and $\varepsilon''_m \ll |\varepsilon_m|$. The film is deposited on the dielectric substrate with the permittivity ε_d and it is covered with a protective dielectric layer ε_e. The thickness $2h$ of the metal film is chosen in such a way that the incident light infiltrate in the substrate. The propagation of SP in the metal film that thickness $2h$ is less than the skin layer can be considered in the quasistatic approximation. In this case the electric field E of SP can be find in terns of the electric potential φ so that $E = -\nabla\varphi$. The electric potential is a solution of the Laplace equation $\triangle\varphi = 0$.

We consider the metal film placed at the plane $z = 0$. SP propagates over the film in x direction with wavevector q. The electric field is invariant under translation in y direction (see Fig. 1). SP field exponentially decays away from PZ. Electric potential φ_e above the film ($z < -h$) equals to $\varphi_e = A\exp(iqx)\exp(qz)$, the potential below film ($z > h$) equals to $\varphi_d = B\exp(iqx)\exp(-qz)$. Inside the metal film ($-h < z < h$) the solution of the Laplace equation has the form $\varphi_m = \exp(iqx)[C_1\exp(qz) + C_2\exp(-qz)]$. To find the electric field E in SP that is the coefficients A, B, C_1, and C_2 we use the boundary conditions

$$E_{e,x} = E_{m,x},\ \varepsilon_e E_{e,z} = \varepsilon_m E_{m,z};\ z = -h, \tag{1}$$

$$E_{d,x} = E_{m,x},\ \varepsilon_d E_{d,z} = \varepsilon_m E_{m,z};\ z = h, \tag{2}$$

where E_e, E_m, and E_d are the electric fields in the protective layer, metal film, and dielectric substrate correspondingly. Equations (1) and (2) have nontrivial solution if and only if the corresponding determinant Det equals to zero. Thus the SP wavevector q is obtained from the equation $Det = 0$

$$q = \frac{1}{4h}\log\left[\frac{(\varepsilon_e - \varepsilon_m)(\varepsilon_d - \varepsilon_m)}{(\varepsilon_e + \varepsilon_m)(\varepsilon_d + \varepsilon_m)}\right]. \tag{3}$$

Recall the optical metal permittivity is mainly negative $\Re\varepsilon_m < 0$. In the limit $|\varepsilon_m| \gg \varepsilon_e, \varepsilon_d$, which is typical for the visible and infrared range, the SP wavevector approximates as

$$q \simeq -\frac{\varepsilon_e + \varepsilon_d}{2h\varepsilon_m} \tag{4}$$

, In any case we suppose that the film thickness $2h$ is much smaller than the SP wavelength that is $hq \ll 1$. Then the electric field inside the metal film E_m does not depend on the normal coordinate "z" and the electric current $J(x)$ is function of "x", which is a solution of the wave equation for SP, namely,

$$\frac{d^2J(x)}{dx^2} + q^2J(x) = q^2\Sigma E_e(x), \tag{5}$$

where the external field E_e is added to the r.h.s. The term Σ in r.h.s. of Eq. (5) is in general a linear operator which gives spatial harmonics of the electric nearfield when the external field E_e is an arbitrary function

of the coordinate "x". To simplify the consideration we take into account the field modulation due to the SP excitation only and approximate as $\Sigma \simeq 2h\sigma_m$, where $\sigma_m - i\dfrac{\omega\varepsilon_m}{4\pi}$ is the metal conductivity. When the spatial scale of the external field $E_e(x)$ is much larger than the plasmon wavelength $\lambda_p = 2\pi/q$ the current $J(x) = 2h\sigma_m E_e(x)$. That is we assume that the film current follows the external field and this approach can be called one mode approximation.

The plane EM wave excites SP in the metal nanostrip that have finite width $2d$ and thickness $2h \ll 2d$. Suppose that the strip is illuminated by the light which is incident under the angel θ in respect to the normal to the x, y plane of the film (see Fig. 1). First we consider the plane of incidence, which is perpendicular to the metal strips, that is the wave vector $k = n_e\omega/c$, ($n_e = \sqrt{\varepsilon_e}$) has x and z components $\mathbf{k} = k\{\sin\theta, 0, -\cos\theta\}$. In P polarized light the incident electric field has component $E_{0,x} = E_0\cos\theta$ and the external electric field in Eq. (5) takes the following form $E_e = E_{0,x}\exp(ik_x x)$, where $E_{0,x}$, and k_x are the projections of the field E_0 and the wave vector $k = n_e\omega/c$ of the impingement light. Assuming that $|\varepsilon_m| \gg \varepsilon_e, \varepsilon_d$ we apply zero boundary condition $J(\pm d) = 0$ at edges of a strip (see discussion in the next section) and Eq. (5) gives

$$J(x) = J_1(x) + J_2(x), \tag{6}$$

where the current

$$J_1(x) = \Sigma_e E_e, \quad \Sigma_e = \frac{2hq^2\sigma_m}{q^2 - k_x^2}, \tag{7}$$

does not depend on the edge boundary conditions, and the current

$$J_2(x) = -E_e\Sigma_e \frac{e^{-ixk_x}\left[e^{iqx}\sin d\,(k_x + q) - e^{-iqx}\sin d\,(k_x - q)\right]}{\sin 2dq} \tag{8}$$

is the current due to the reflection of the plasmon from edges of the strip.

The PS wavevector $q = q_1 + iq_2$ is in general a complex value, where the imaginary part q_2 estimates from Eq. (3) as

$$q_2 = \frac{\varepsilon_m''\left(\varepsilon_d + \varepsilon_e\right)\left(\varepsilon_m'^2 - \varepsilon_d\varepsilon_e\right)}{2h\left(\varepsilon_m'^2 - \varepsilon_d^2\right)\left(\varepsilon_m'^2 - \varepsilon_e^2\right)}. \tag{9}$$

It is easy to check that $q_2/q_1 \sim \varepsilon_m''/|\varepsilon_m| \ll 1$. We obtain from Eq. (8) "odd" plasmon resonances where $q_1^{(od)}d = (\pi/2)m,\ m = 1, 3, 5\ldots$ and "even" resonances where $q_1^{(ev)}d = (\pi/2)m,\ m = 2, 4, 6\ldots$. The electric field $E_{\max}$ in even and odd SP resonance estimates as

$$E_{\max}^{od} = -E_{0,x}\frac{2i^m q_1^3}{\pi m q_2\left(k_x^2 - q_1^2\right)}\cos\left(q_1 x\right)\cos\left(\frac{\pi m k_x}{2q_1}\right) \tag{10}$$

and

$$E_{\max}^{ev} = E_{0,x}\frac{2i^m q_1^3}{\pi m q_2\left(k_x^2 - q_1^2\right)}\sin\left(q_1 x\right)\sin\left(\frac{\pi m k_x}{2q_1}\right) \tag{11}$$

correspondingly. Since we consider narrow strips where $d \ll \lambda$, i.e., $q_1 \gg k_x$ the odd resonances estimate as $|E_{\max}^{ev}/E_{0,x}| \sim |k_x/q_2|$ and it is much less than the even resonances $|E_{\max}^{ev}/E_{0,x}| \sim q_1/q_2 \sim |\varepsilon_m'/\varepsilon_m''| \gg 1$. When the light is impinged normal to the thin metal strip, i.e., $k_x = 0$ the even resonances get excited only. In S polarization when the electric field is perpendicular to the plane of incidence the external electric field $\{0, E_0, 0\}$ is aligned with the strip direction. Then the current $J_y = \Sigma_e E_0$ flows along continuous nanothin metal strip.

For example, we consider the strip embedded in the dielectric host with permittivity $\varepsilon_e = \varepsilon_d$. The condition for the first resonance $qd = \pi/2$ can be rewritten by substituting the wavevector q from Eq. (4), obtaining $\dfrac{\varepsilon_m h}{\varepsilon_d d} = \dfrac{2}{\pi}$. This result close to the well known quasistatic result for the plasmon resonance in the prolate metal $2D$ ellipsoid (semi-axes $h \ll d$) which resonates when $\dfrac{\varepsilon_m h}{\varepsilon_d d} = 1$ (see, e.g., [30]).

The similar consideration holds when $\{y, z\}$ is the plane of incidence. That is EM wave is impinged along the strip. In this case S polarized EM wave excites SP since the S electric field is directed across the strip whereas the resonance conditions remains the same. Thus we obtain that the natural light, which contains EM waves with various polarization, excites SP in a metal strip for any direction of the incidence. Above equations are derived for a single metal strip.

Consider now PZ composed from the periodic system of the parallel metal nanostrips. It is still assumed that the strip thickness $2h$ is much less than the skin depth so the electric field does not depend on the coordinate z in the metal strip. Recall the width of a strip equals $2d$, the gap between neighboring

strips equals to $2g$ (see schematic Fig. 3), so the PZ period equals to $2d + 2g < \lambda/2$. Conductance of PZ is anisotropic: The conductance in y direction equals to $\Sigma_{yy} = \Sigma_e p$, where $p = d/(d + g)$ is the part of the $z = 0$ interface, which is covered by the metal strips, the surface conductance Σ_e is given by Eq. (6).

To find the conductance Σ_{xx} across the strips it is necessary to find the electric current when the transverse external field E_e is applied. The current inside the strip is still given by Eq. (6). However, the current $J(x)$ does not now vanish at the edges of the strip since two neighboring strips have the capacity connection. The interstrip capacitance connects neighboring metal strips that results in collective response of

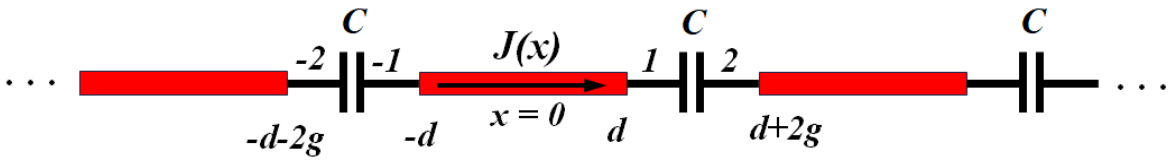

Рис. 3: Lumped circuit of plasmon zebra with period $2d+2g$; electric current $J(x)$ flows in metal nanostrips that are connected via interstrip capacitance C.

PZ to the external field. The interstrip capacitance C shown in Fig. 3 we approximate as capacitance between two thin strips made of perfectly conducting metal. Two perfectly conducting strips are placed at interface $z = 0$ between upper half space $z > 0$ with permittivity ε_e and lower half -space $z < 0$ with permittivity ε_d. First perfect strip has width $2d$ and it is centered at the origin of the coordinate. Second perfectly conducting also has width $2d$ and its center is at the coordinate $x = 2(d + g)$. The gap between right and left edges of the strips equal $2g$. To find the capacitance C we suppose left strip has the electric charge Q and right strip has charge $-Q$. Then the electric field is elementary found from complex variable theory. We introduce the complex variable $u = x - d - g + iz$, then the complex electric field $E_g(u) = E_{gx}(u) + iE_{gy}(u)$ equals to

$$E_g(u) = E_{gx}(u) - iE_{gz}(u) = \frac{E_{0g}\, d(2d + g)}{\sqrt{(d^2 - u^2)((2d + g)^2 - u^2)}}, \tag{12}$$

where E_{gx} and E_{gz} take real values that are proportional to the charge Q. The complex electric field E_g is an analytical function. Therefore their components $E_{gx}(u)$ and $E_{gz}(u)$ are solutions of the Laplace equation. The branch of the analytical function $E_g(u)$ is chosen so that $E_g(0) = E_{0g}$. The electric field E_g has only "z" component on the surface of the metal plates. Therefore, the electric charge equals to

$$Q_1 = i\alpha \int_{-2d-g}^{-g} E_g(u)\, du = E_{0g}\alpha g K\left(\frac{4d(d + g)}{(2d + g)^2}\right) \simeq E_{0,g}\alpha g \log\left(\frac{8d}{g}\right) \tag{13}$$

for the electric field E_g given by Eq. (12), where $\alpha = \dfrac{\varepsilon_e + \varepsilon_d}{4\pi}$. The last esteem holds for the narrow slit between the strips when $g \ll d$. The electric charge Q_2 on the right strip has the opposite sign $Q_2 = -Q_1$.

The electric field E_g has x component only in the gap $-g < u < g$ between the metal plates. The electric field E_s at the edge of the strip is estimated assuming that the strip thickness $2h$ is much smaller than the gap width, i.e., $g \gg h$. Strictly speaking the field given by Eq. (12) goes to infinity exactly at the edges where $u = \pm g$. Since a metal strip has the finite thickness $2h$ we substitute the coordinate $u_{1,2} = \pm(g - 2h)$ in Eq. (12) obtaining

$$E_{1,2} = E_g(u_{1,2}) = \mp E_{0,g}\frac{(2d + g)}{4\sqrt{d(d + g)}}\sqrt{\frac{g}{h}}, \tag{14}$$

where the condition $g \gg h$ is taken into account. The current flows out of the edge u_2 equals to $J_2 = (\sigma_e + \sigma_d)hE_2$, where $\sigma_{e,d} = -i\dfrac{\omega\varepsilon_{e,d}}{4\pi}$. The ratio of the derivative of the charge with respect to time $-dQ/dt = i\omega Q_1$ to the current J equals to

$$N = -4\frac{\sqrt{d(d + g)}}{(2d + g)}\sqrt{\frac{g}{h}}K\left(\frac{4d(d + g)}{(2d + g)^2}\right). \tag{15}$$

It is a dimensionless quantity, which depends on the geometry of the system, namely, the strip width $2d$, strip thickness $2h$ and the gap $2g$ between the neighboring trips.

On the other hand the electric charge Q at the edge of the strip (see Fig. 3) estimates from the charge conservation law as $Q \sim \dfrac{l}{i\omega}\dfrac{dJ(x)}{dx}\Big|_{x=d}$, where the current $J(x)$ is given by Eq. (5), l is the characteristic length for the charge distribution. The capacity connection between the metal strips in PZ is important at the plasmon resonances when the number of maxima of the current $|J(x)|$ equals to the order m of the

resonance. Then the length l could be estimated as $l \sim d/m$, where $m = 1, 2, 3, \ldots$ is the order of the resonance. We obtain the following boundary condition for the electric current at the strip edges.

$$\left.\frac{d}{J(x)}\frac{d\,J(x)}{dx}\right|_{x=d} = -\left.\frac{d}{J(x)}\frac{dJ(x)}{dx}\right|_{x=-d} = \gamma m N = -\beta, \tag{16}$$

where γ is a numerical coefficient. The value of γ cam be obtained by comparison with computer simulation. Bellow, to simplify consideration, we put $\gamma \approx 1$. The important parameter β approximates as $\beta \simeq 2\pi\sqrt{d/h}$ for the isolated strips when the gap $g \gg d$. It is independent on the gap value g and much larger than one $\beta \gg 1$, which corresponds to the boundary conditions $J(\pm d) = 0$ used in the previous section. In the opposite case of a narrow slit between the strips $g \ll d$ the boundary parameter $\beta \simeq 2\sqrt{\frac{g}{h}}\log\left(\frac{8d}{g}\right)$ so it is again much larger than one since we consider narrow strips which thikness $h \ll g, d$.

The plasmon current is obtained from the solution of Eq. (5) with Eq. (16) boundary conditions

$$J(x) = J_1(x) + J_2(x), \quad J_2(x) = -E_e\Sigma_e\frac{A(q)e^{iqx} - A(-q)e^{-iqx}}{2D_1(q)D_2(q)}, \tag{17}$$

$$A(q) = \left(\beta^2 - d^2 q k_x\right)\sin\left(d\left(k_x + q\right)\right) + \beta d\left(k_x + q\right)\cos\left(d\left(k_x + q\right)\right), \tag{18}$$

$$D_1(q) = \beta\cos(dq) - dq\sin(dq), \quad D_2(q) = \beta\sin(dq) + dq\cos(dq), \tag{19}$$

where the current $J_1(x)$ and the conductance Σ_e are given by Eq. (7). The plasmon current $J(x)$ has evident resonance when the projection of the wavevector k_x of the incident light equals to the plasmon wavevector $\Re q = k_x$. It could happen in so-called Kretschmann geometry where the upper half space ($z < 0$) permittivity ε_e is larger than the lower half-space permittivity $\varepsilon_e > \varepsilon_d$ and also the angle of incidence θ (see Fig. 1) is large enough so that $k_x = \sin\theta\,\frac{\omega}{c}\sqrt{\varepsilon_e} = q$. Then EM wave, which is incident from above, excites plasmon in a metal film.

Yet, we consider in this paper the EM that propagating in all the space. The resonance can happen for any k_x, i.e., for any incident wave when the discriminant $D_1(q)D_2(q)$ in Eq. (17) vanishes. Consider the plasmon electric field of the first order resonance where $m = 1$. To simplify the consideration we assume that $k_x = 0$ that is the light is incident normal to the PZ plane, i.e. $z = 0$ plane. Then the dimensionless plasmon electric field $|E(x)|^2 = |J(x)/(E_e 2h\sigma_m)|^2$ reaches its maximum at the centers of PZ strips. Substituting the plasmon current from Eq. (17) we obtain

$$|E(0)|^2 = \left|1 - \frac{\beta}{D_1(q)}\right|^2 \tag{20}$$

The real part of the discriminant D_1 vanishes exactly at the resonance when $D_1(q = q_r) = 0$, $q_r = q_{r1} + iq_{r2}$. Expanding $D_1(q_r)$ in series of q_{r2} we obtain the maximum resonance field

$$|E_{max}|^2 \simeq \frac{\beta^4}{d^2 q_{r2}^2\left(\beta^2 + \beta + d^2 q_{r1}^2\right)^2\sin\left(dq_{r1}\right)^2} \tag{21}$$

The wavelength λ_p of the plasmon is on the order of the width $2d$of a strip, that is $dq_{r1} \sim d/\lambda \sim 1$ in the resonance. On the other hand the parameter β given by Eq. (16) is proportional to $\beta \sim 1/\sqrt{g/h}$ and it could be rather large for a thin metal film, where the thickness h is much smaller than the inter strip gap $g \gg h$. The dispersion equation $D_1(q_{r1}) = 0$ is expanded in reciprocal powers of β, which gives

$$q_{r1} = \frac{\pi}{2d}\left(1 - \beta^{-1} + \beta^{-2}\right), \tag{22}$$

and the maximum field estimates as $E_{\max} \sim 1/(dq_{r2})^2$. Substituting here imaginary part q_{r2} from Eq. (9) we obtain the following

$$|E_{max}|^2 \simeq \frac{4h^2\left(\varepsilon_m'^2 - \varepsilon_d^2\right)^2\left(\varepsilon_m'^2 - \varepsilon_e^2\right)^2}{\varepsilon_m''^2 d^2\left(\varepsilon_d + \varepsilon_e\right)^2\left(\varepsilon_m'^2 - \varepsilon_d\varepsilon_e\right)^2} \sim \frac{\varepsilon_m'^4}{\varepsilon_m''^2}\left(\frac{2h}{d\left(\varepsilon_d + \varepsilon_e\right)}\right)^2, \tag{23}$$

where the last esteem holds for red and infrared spectral range where the metal permittivity is typically large $|\varepsilon_m| \gg 1$. For example, the silver permittivity estimates as $\varepsilon_{Ag} \simeq -30 + i0.38$ [31], therefore, the factor $\varepsilon_m'^4/\varepsilon_m''^2 > 10^6$ is huge in Eq. (23). Note the electric field enhancement in metal nanoparticles is typically restricted by the radiation loss that rapidly increases with the particle size. Yet, a radiation loss is almost zero for the fully periodic PZ, the radiation loss happens due to the manufacturing imperfections only. We speculate that the result for the huge resonance field enhancement obtained above in quasistatic approximation holds up to diffraction limit. The electric field E_{max} in PZ is shown in Fig. 4. It can be observed that local electric field can be enhanced in PZ for any part of visible spectrum.

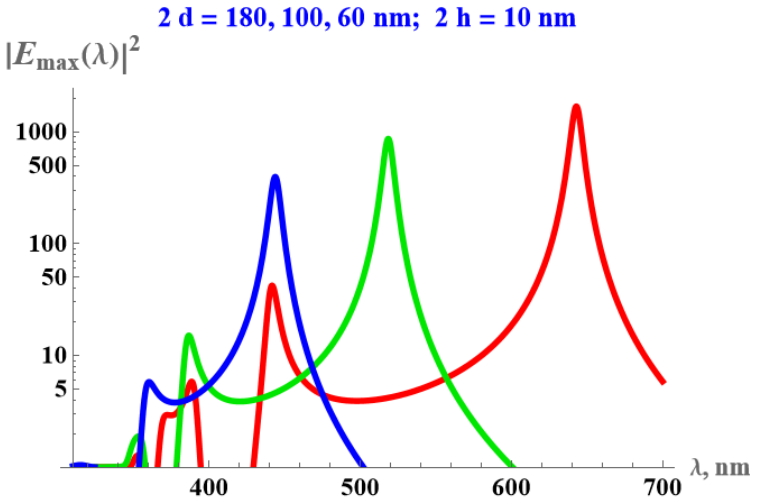

Рис. 4: Electric field enhancement in PZ illuminate by light impinged normal to PZ plane; metal strip thickness $2h = 10\,nm$, interstrip gap $2g = 40\,nm$, strip width $2d = 180, 100, 60\,nm$ (red, green, blue); amplitude of incident light $E_0 = 1$.

3. Reflectance and Color of Plasmon Zebra

It is save to suppose that even thin PZ effectively reflects the light, which wavelength correspond to the plasmon resonance. That is the color of PZ corresponds to the resonance wavelength. The reflectance of PZ is defined by its effective surface conductance $\Sigma^{(ef)}$, which is anisotropic in this case $\Sigma^{(ef)} = \{\Sigma_x, \Sigma_y\}$. The effective surface conductance is obtained by average of the electric current over the PZ plane $\Sigma_x = p\int_{-d}^{d} J(x)/E(x)\,dx/2d$, $\Sigma_y = p\Sigma_e$, where $p = d/(d+g)$ is the fraction of $z = 0$ plane, which is covered by the metal strips. Integration of the electric current given by Eq. (17) gives the effective x conductance

$$\Sigma_x = p\Sigma_e \left[\frac{\sin dk_x}{dk_x} + \frac{\sin dq\,(dk_x \sin dk_x - \beta\cos dk_x)}{dqD_1(q)}\right], \tag{24}$$

which resonates as it is shown in Fig. 5. The PZ permittivity resonate when the discriminant $D_1(q) \simeq 0$, i.e., for the odd plasmon resonances. In this sense the even resonances ($D_2(q) = 0$) are so-called dark resonances [32].

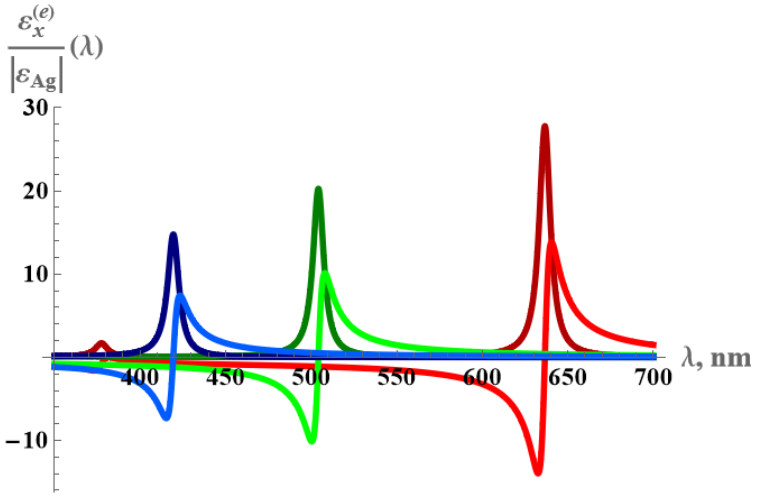

Рис. 5: Ratio of real and imaginary parts of the effective zebra permittivity $\varepsilon_x^{(e)} = \varepsilon_x^{\prime(e)} + i\varepsilon_x^{\prime\prime(e)}$ to silver permittivity ε_{Ag}; red and dark red strip width $2d = 180\,nm$, green and dark green $2d = 100\,nm$, blue and dark blue $2d = 60\,nm$; metal strip thickness $2h = 10\,nm$, interstrip gap $2g = 40\,nm$.

We consider here, for simplicity, the case when the natural light is incident normal to the plane of PZ. The reflectance r of a thin metal film, which thickness is less than the skin depth, is defined by the surface conductance (see, e.g., [33, 34]) or effective surface permittivity $\varepsilon^{(ef)} = -i2\pi\Sigma^e/h\omega$. The effective surface permittivity is anisotropic $\varepsilon^e = \left\{\varepsilon^e_x, \varepsilon^e_y\right\}$ for a PZ. Recall we consider PZ composed of parallel metal strips, which are aligned with y axis as it is shown in Fig. 1. The reflectance r is obtained by matching the incident EM wave in the upper half space, where the electric field $E_e \sim E_0\left[\exp(ik_e z) + r\,\exp(-ik_e z)\right]$ and the transmitted wave in the lower half space $E_d \sim E_0 t\exp(ik_d z)$, where t is the transmittance of PZ; wavevectors of the incident and transmittance waves equal to $k_e = n_e k$ and $k_d = n_d k$, where $n_e = \sqrt{\varepsilon_e}$ and $n_d = \sqrt{\varepsilon_d}$. That is we extrapolate EM field to PZ surface, i.e., to the plane $z = -h$ (see Fig. 1). By the same token we extrapolate farfield in the lower half space $E_d \sim E_0 t\exp(ik_d z)$ to the lower PZ boundary $z = h$. Among all EM spatial harmonics excited in PZ we take into account those that are due to the plasmon resonance. The field of SP is added to the fields E_e and E_d. This approach is similar to GOL method [21, 22] and can be called one mode GOL approximation.

The vector of the electric field $E_0 = \{E_{0x}, E_{0y}, E_{0z},\}$ is determined by the polarization of the incident light. To find the reflectance r and transmittance t of a thin film we equate the electric field of the incident light, electric field in the film, and the field in the transmitted light in the middle of the film at the plane $z = 0$. The reflectance r is defined by the polarization of the incident light when the direction of EM wave is normal to the film. Then solution of the Maxwell equations and matching the magnetic fields at the interfaces of the film gives

$$r_{x,y} = \frac{n_e - n_d + W_{x,y}\left(\varepsilon^e_{x,y} - n_d n_e\right)}{n_d + n_e - W_{x,y}\left(\varepsilon^e_{x,y} + n_d n_e\right)}, \tag{25}$$

where

$$W_{x,y} = i\tan\left(2hk\sqrt{\varepsilon^e_{x,y}}\right)/\sqrt{\varepsilon^e_{x,y}}, \tag{26}$$

where the effective surface permittivity $\varepsilon^e_{x,y} = i\dfrac{2\pi}{\omega h}\left\{\Sigma_x, \Sigma_y\right\}$ is obtained from Eq. (24), wavevector $k = \omega/c$. The reflectance of PZ is shown in Fig. 6. The maxima of the reflectance correspond to the maxima of the effective PZ permittivity (Fig. 5). Note the reflectance of PZ with the strip width of 200 nm has two maxima

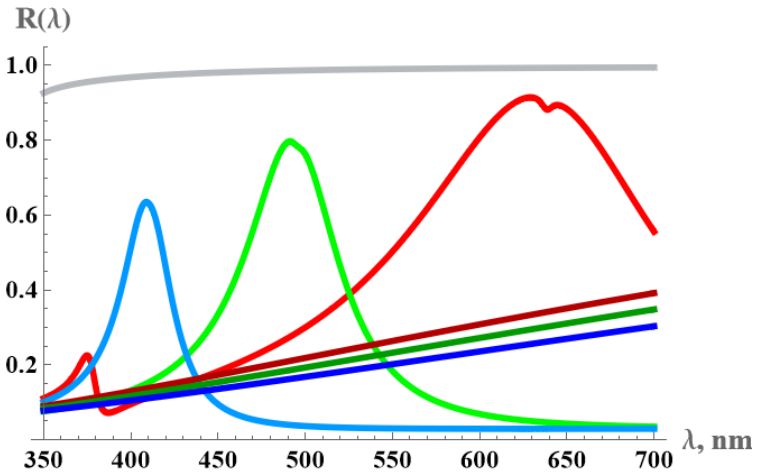

Рис. 6: Reflectance of silver zebra with thickness $2h = 10\,nm$, interstrip gap $2g = 40\,nm$, that is deposited on glass substrate $\varepsilon_e = 1$, $\varepsilon_d = 2$; red and dark-red are x and y reflectances of PZ with strip width $2d = 180\,nm$, green and dark-green are x and y reflectances with width $2d = 100\,nm$, blue and dark-blue are x and y reflectances with width $2d = 60\,nm$; gray line is reflectance of bulk silver plate.

that correspond to the first $m = 1$, $\lambda \simeq 650\,nm$ and third $m = 3$, $\lambda \simeq 370\,nm$ plasmon resonances.

The reflectance of PZ is anisotropic as well as surface conductivity as it is shown in Figs. 5 and 6. We consider the color of PZ when it is illuminated by the natural light, which is composed from EM of various polarization. We assume that photons of different polarization are incoherent. Therefore, the total reflection coefficient being averaged over the polarization equals to $R(\lambda) = \left(|r_x(\lambda)|^2 + |r_y(\lambda)|^2\right)/2$. We are interested in the PZ color, which is determined by behavior the reflection $R(\lambda)$ as function of the wavelength. The coloring is well established problem discussed, for example, in the recent papers [19, 35–38].

Yet, everybody sees her/his own a color shadow. For qualitative consideration we adopt the simplest possible approach. All visible spectrum is divided on three parts: red $\lambda_{G1} < \lambda < \lambda_R$, green $\lambda_{G2} < \lambda < \lambda_{G1}$, and blue $\lambda_B < \lambda < \lambda_{G2}$, where $\lambda_R = 680\ nm$, $\lambda_{G1} = 590\ nm$, $\lambda_{G2} = 480\ nm$, and $\lambda_B = 390\ nm$. We calculate the {**R**,**G**,**B**} color as $\mathbf{R} = W_1 \int_{\lambda_{G1}}^{\lambda_R} R(\lambda)\, d\lambda$, $\mathbf{G} = W_2 \int_{\lambda_{G2}}^{\lambda_{G1}} R(\lambda)\, d\lambda$, and $\mathbf{B} = W_3 \int_{\lambda_{G1}}^{\lambda_R} R(\lambda)\, d\lambda$, where the color weights W_1, W_2, and W_3, are chosen to mimic real color. We consider here the silver PZ, then the color weights $\{W1, W2, W3\} = \{0.80, 0.83, 0.85\}$ are chosen in such a way that {**R**,**G**,**B**} color of the bulk silver, calculated from the reflectance in Fig. 6 has the silver color indeed as it is shown in Fig. 7. The silver PZ

Рис. 7: Color of silver zebra with thickness $2h = 10\,nm$, interstrip gap $2g = 40\,nm$, that is deposited on glass substrate $\varepsilon_e = 1$, $\varepsilon_d = 2$; 1, 2, 3 – color of PZ with strip width $2d = 200\,nm$, $2d = 120\,nm$, and $2d = 80\,nm$, 4–bulk silver plate.

has various colors in Fig. 7 that depends of the parameters that can be easily changed in the process of the manufacturing. Yet, thus obtained plasmon colors are not pure enough since the PZ reflectance has rather wide maxima at resonance wavelength.

4. Conclusions

The simple analytical theory is presented for the plasmon resonances in the system of thin periodical metal strips and patches. In particular plasmon resonance are analytically calculated for the system of parallel metal strips we called plasmon zebra (PZ). The frequencies of the plasmon resonances correspond to the maxima of PZ reflectance. Simple PZ with all the strips of the same width gives RGB colors. Combination the metal strips of different parameters could produce the plasmon painting of arbitrary color.

5. Funding

The work supported by the Russian Science Foundation under grant 23-19-00788, https://rscf.ru/project/23-19-00788/.

Список литературы

[1] The Lycurgus Cup - a Roman nanotechnology / Freestone I., Meeks N., Sax M., and Higgitt C. // Gold Bull. — 2007. — Vol. 40. — P. 270.

[2] PerezVillar S., Rubio J., Oteo J. L. Study of color and structural changes in silver painted medieval glasses // J Non Cryst Solids. — 2008. — Vol. 354. — P. 1833.

[3] Ali H. Biodegradation of synthetic dyes // Water Air Soil Pollut. — 2010. — Vol. 213. — P. ,251.

[4] Plasmonic colour generation / Kristensen A., Yang J. K. W., Bozhevolnyi S. I., Link S., Nordlander P., Halas N. J., and Mortensen N. A. // Nat. Rev. Mater. — 2016. — Vol. 2. — P. 16088.

[5] Colors with plasmonic nanostructures: A full-spectrum review / Song M., Wang D., Pana S., Choudhury S., Nyga P., Kudyshev Z. A., Yu H., Boltasseva A., Shalaev V. M., and Kildishev A. V. // Appl. Phys. Rev. — 2019.

[6] Structural color generation: from layered thin films to optical metasurfaces / Wang D., Liu Z., Wang H., Li M., Guo L. J., and Zhang C. // Nanophotonics. — 2023. — Vol. 12. — P. 1019.

[7] Printing colour at the optical diffraction limit / Kumar K., Duan H., Hegde R. S., Koh S. C. W., Wei J. N., and Yang J. K. W. // Nat. Nanotechnol. — 2012. — Vol. 7. — P. 557.

[8] Reflective plasmonic color filters based on lithographically patterned silver nanorod arrays / Si G., Zhao Y., Lv J., Lu M., Wang F., Liu H., Xiang N., Huang T. J., Danner A. J., Teng J., and Liu Y. J. // Nanoscale. — 2013. — Vol. 5. — P. 6243.

[9] Subwavelength plasmonic color printing protected for ambient use / Roberts A. S., Pors A., Albrektsen O., and Bozhevolnyi S. I. // Nano Lett. — 2014. — Vol. 14. — P. 783.

[10] Plasmonic color palettes for photorealistic printing with aluminum nanostructures / Tan S. J., Zhang L., Zhu D., Goh X. M., Wang Y. M., Kumar K., Qiu C. W., and Yang J. K. W. // Nano Lett. — 2014. — Vol. 14. — P. 4023.

[11] Plasmonic colour laser printing / Zhu X., Vannahme C., Hojlund-Nielsen E., Mortensen N. A., and Kristensen A. // Nat. Nanotechnol. — 2015. — Vol. 11. — P. 325.

[12] Comparative study of plasmonic colors from all-metal structures of posts and pits / Goh X. M., Ng R. J. H., Wang S., Tan S. J., and Yang J. K. W. // ACS Photonics. — 2016. — Vol. 3. — P. 1000.

[13] Nanophotonic structural colors / Ng R. J. H., Krishnan R. V., Wang H., and Yang J. K. W. // Nanophotonics. — 2020. — Vol. 9. — P. 533.

[14] A plasmonic painters method of color mixing for a continuous red-green-blue palette / Hail C. U., Schnoering G., Damak M., Poulikakos D., and Eghlidi H. // ACS Nano. — 2020. — Vol. 14. — P. 1783.

[15] Wang H. C., Martin O. J. F. Polarization-controlled chromo-encryption // Adv. Opt. Mater. — 2023. — Vol. 11, no. 2202165.

[16] Lochbihler H. Colored images generated by metallic sub-wavelength gratings // Opt. Express. — 2009. — Vol. 17. — P. 12189.

[17] Plasmonic nanoresonators for high-resolution colour filtering and spectral imaging / Xu T., Wu Y.-K., Luo X., and Guo L. J. // Nat. Commun. — 2010. — Vol. 1. — P. 59.

[18] Structural color printing based on plasmonic metasurfaces of perfect light absorption / Cheng F., Gao J., Luk T. S., and Yang X. // Sci. Rep. — 2015. — Vol. 5. — P. 11045.

[19] Wide-range angle-sensitive plasmonic color printing on lossy-resonator substrates / Chowdhury S. N., Simon J., Nowak M. P., Pagadala K., Nyga P., Fruhling C., Bravo E. G., Mackowski S., Shalaev V. M., Kildishev A. V., and Boltasseva A. // Adv. Optical Mater. — 2023. — P. 2301678.

[20] Genov D. A., Sarychev A. K., Shalaev V. Metal-dielectric composite filters with controlled spectral windows of transparency // Journal of Nonlinear Optical Physics and Materials. — 2003. — Vol. 12, no. 4. — P. 1.

[21] Sarychev A. K., Bergman D. J., Yagil Y. Theory of the Optical and Microwave Properties of Metal-Dielectric Films, // Phys. Rev. B. — 1995. — Vol. 51. — P. 5366.

[22] Barbillon G., Ivanov A., Sarychev A. K. Hybrid Au/Si disk-shaped nanoresonators on gold film for amplified SERS chemical sensing // Nanomaterials. — 2019. — Vol. 9. — P. 1588. — Access mode: https://doi.org/10.3390/nano9111588.

[23] Enhancement of local electromagnetic fields by periodic optical resonators / Sarychev A. K., Ivanov A. V., Afanasyev K. N., Bykov I. V., Boginskaya I. A., Kurochkin I. N., Lagarkov A. N., Merzlikin A. M., Mikheev V. V., Negrov D. V., Ryzhikov I. A., and Sedova M. V. // Quantum Electronics. — 2018. — Vol. 48. — P. 1147.

[24] Metal-dielectric optical resonance in metasurfaces and SERS effect / Sarychev A. K., Bykov I. V., Boginskaya I. N., Ivanov A. V., Kurochkin I. N., Lagarkov A. N., Nechaeva N. L., and Ryzhikov I. A. // Optical and Quantum Electronics. — 2019. — Vol. 52.

[25] Light Concentration by Metal-Dielectric Micro-Resonators for SERS Sensing / Sarychev A. K.,

Ivanov A., Lagarkov A., and Barbillon G. // Materials. — 2019. — Vol. 12, no. 1. — P. 103.

[26] Silicon-silver metasurface based on regular bars as an effective SERS substrate / Ivanov A. V., Sarychev A. K., Bykov I. V., Boginskaya I. A., Lagarkov A. N., Ryzhikov I. A., Nechaeva N. L., and Kurochkin I. N. // Journal of Phys. Conf. Ser. — 2020. — Vol. 1461. — P. 012057.

[27] SERS for bacteria, viruses, and protein biosensing / Kurochkin I. N., Eremenko A. V., Evtushenko E. G., Nechaeva N. L., Durmanov N. N., GulievIlya R. R., Ryzhikov I. A., Boginskaya I. A., Sarychev A. K., Ivanov A. V., and Lagarkov A. N. // Macro, Micro, and Nano-Biosensors, / ed. by Rai M., Reshetilov A., Plekhanova Y., Ingle A. P. — Springer. — 2021. — P. 75–94.

[28] Multiscale flaked silver SERS-substrate for glycated human albumin biosensing / Nechaeva N. L., Boginskaya I. A., Ivanov A. V., Sarychev A. K., Eremenko A. V., Ryzhikov I. A., Lagarkov A. N., and Kurochkin I. N. // Anal. Chim. Acta. — 2020. — Vol. 1100. — P. 250–257. — Access mode: https://doi.org/10.1016/j.aca.2019.11.072.

[29] Label-free detection of the receptor-binding domain of the SARS-CoV-2 spike glycoprotein at physiologically relevant concentrations using surface-enhanced raman spectroscopy / Sarychev A. K., Sukhanova A., Ivanov A. V., Bykov I. V., Bakholdin N. V., Vasina D. V., Gushchin V. A., Tkachuk A. P., Nifontova G., Samokhvalov P. S., Karaulov A., and Nabiev I. // Biosensors. — 2022. — Vol. 12, no. 5. — P. 300. — Access mode: https://www.mdpi.com/2079-6374/12/5/300.

[30] Landau L. D., Lifshitz E. M., Pitaevskii L. P. Electrodynamics of continuous media. — 2 ed. — Oxford : Elsevier in Amsterdam, Boston, 1993.

[31] Johnson P. B., Christy R. W. Optical constants of the noble metals // Phys. Rev. B. — 1972. — Vol. 6, no. 12. — P. 4370–4379.

[32] Stockman M. I., Faleev S. V., Bergman D. J. Localization versus delocalization of surface plasmons in nanosystems: can one state have both characteristics? // Phys. Rev. Lett. — 2001. — Sep. — Vol. 87, no. 16. — P. 1–4. — Access mode: http://link.aps.org/doi/10.1103/PhysRevLett.87.167401.

[33] Yagil Y., Yosefin M., Bergman D. J., Deutscher G., and Gadenne P. // Phys. Rev. B. — 1991. — Vol. 43. — P. 11342.

[34] Yagil Y., Gadenne P., Julien C., and Deutscher G. // Phys. Rev. B. — 1992. — Vol. 46. — P. 2503.

[35] Structural colors in metasurfaces: principle, design and applications / Yang B., Cheng H., Chen S., and Tian J. // Mater. Chem. Front. — 2019. — Vol. ,3. — P. 750.

[36] Versatile full-colour nanopainting enabled by a pixelated plasmonic metasurface / Song M., Feng L., Huo P., Liu M., Huang C., Yan F., Lu Y.-q., and Xu T. // Nature Nanotechnology. — 2023. — Vol. 18. — P. 71.

[37] Influence of structural disorder on plasmonic metasurfaces and their colors a coupled point dipole approach: tutorial / Herkert E., Sterl F., Both S., Tikhodeev Sergei G., Weiss T., and Giessen H. // Journal of the Optical Society of America B. — 2023. — Vol. 40. — P. B59.

[38] Novel plasmonic metamaterials based on metal nano-hemispheres and metal-dielectric composites / Niguma R., Matsuyama T., Wada K., and Okamoto K. // Photonics. — 2024. — Vol. 11. — P. 356.

ЗЕБРА-ПЛАЗМОННЫЕ РЕЗОНАНСЫ И НАНОКРАСКА

А. К. Сарычев[1*], А.В. Иванов[1], Д. Бергман[2], Р. Фан[3], А.Ф. Смык[4]

[1] Федеральное государственное бюджетное учреждение науки Институт теоретической и прикладной электродинамики Российской академии наук, Москва, Россия
[2] Тель-Авивский университет, Израиль
[3] Колледж наук об океане и инженерии, Шанхайский морской университет, Шанхай, Китай
[4] ООО «Джеймс Ривер Бранч», Москва, Россия
[*] sarychev_andrey@yahoo.com

Аннотация

Мы исследуем металл-диэлектрические метаповерхности, состоящие из периодических металлических нанополосок, нанесенных на диэлектрическую подложку. Метаповерхность можно назвать плазмонной зеброй (ПЗ). Метаповерхность работает как набор открытых плазмонных резонаторов. Разработана теория плазмона, возбуждаемого в открытых резонаторах, соединенных между собой. Предсказано большое локальное электромагнитное поле для оптических частот, соответствующих возбуждению плазмона. Отражательная способность ПЗ значительно усиливается на частоте плазмонного резонанса, и ПЗ приписывают цвет, соответствующий резонансной частоте. Мы предлагаем ПЗ как простейшую, но легко настраиваемую плазмонную нанокраску.

Ключевые слова: зебра-плазмонный резонанс, усиление электромагнитного поля, нанокраска